USGS
science for a changing world

RESULTS FROM GEOTHERMAL LOGGING, AIR AND CORE-WATER CHEMISTRY SAMPLING, AIR-INJECTION TESTING, AND TRACER TESTING IN THE NORTHERN GHOST DANCE FAULT, YUCCA MOUNTAIN, NEVADA, NOVEMBER 1996 TO AUGUST 1998

4/24/00

Water-Resources Investigations Report 99–4210

U.S. Department of the Interior
U.S. Geological Survey

Prepared in cooperation with the
NEVADA OPERATIONS OFFICE
U.S. DEPARTMENT OF ENERGY
Interagency Agreement DE-AI08-97NV12033

Results from Geothermal Logging, Air and Core-Water Chemistry Sampling, Air-Injection Testing, and Tracer Testing in the Northern Ghost Dance Fault, Yucca Mountain, Nevada, November 1996 to August 1998

By Gary D. LeCain, Lawrence O. Anna, and Michael F. Fahy

U.S. GEOLOGICAL SURVEY

Water-Resources Investigations Report 99–4210

Prepared in cooperation with the
NEVADA OPERATIONS OFFICE
U.S. DEPARTMENT OF ENERGY
Interagency Agreement DE–AI08–97NV12033

Denver, Colorado
2000

U.S. DEPARTMENT OF THE INTERIOR
BRUCE BABBITT, Secretary

U.S. GEOLOGICAL SURVEY
Charles G. Groat, Director

Trade names: SEAMIST, FRACMAN, CLUSTRAN

The use of firm, trade, and brand names in this report is for identification purposes only and does not constitute endorsement by the U.S. Geological Survey.

For additional information write to:

Chief, Earth Science Investigations Program
Yucca Mountain Project Branch
U.S. Geological Survey
Box 25046, Mail Stop 421
Denver Federal Center
Denver, CO 80225-0046

Copies of this report can be purchased from:

U.S. Geological Survey
Information Services
Box 25286
Federal Center
Denver, CO 80225

CONTENTS

FIGURES

TABLES

CONVERSION FACTORS, ABBREVIATIONS, AND VERTICAL DATUM

Multiply	By	To obtain
centimeter (cm)	0.394	inch
cubic meter (m^3)	35.341	cubic foot
cubic meter per second (m^3/s)	15,852.0	gallon per minute
kilogram per cubic meter (kg/m^3)	0.062	pound per cubic foot
kilogram per cubic meter per second ($kg/m^3/s$)	3.72	pound per cubic foot per minute
kilometer (km)	0.6214	mile
kilopascal (kPa)	0.145	pound-force per square inch
liter (L)	0.264	gallon
meter (m)	2.281	foot
square meter (m^2)	10.765	square foot
square meter per second (m^2/s)	645.9	square foot per minute
meter per second (m/s)	196.850	foot per minute
micrometer (μm)	3.94×10^{-7}	inch
millimeter (mm)	0.0394	inch
Pascal (Pa)	1.45×104	pound-force per square inch
Pascal second (Pa×s)	10.0	poise
standard liter per minute (sLpm)*	0.2642	gallons per minute

*In this report, the term standard means a measurement taken at a temperature of 0 degree Celsius and atmospheric pressure of 101.3 kilopascals.

TU is tritium unit and corresponds to one ^3H atom per $^{10}18$ atoms of hydrogen.

Temperature in degree Celsius (°C) can be converted to degree Fahrenheit (°F) as follows:

$$°F = 1.8\ (°C) + 32$$

The permeability equations use kelvin. To convert kelvin (K) to degrees Fahrenheit (°F) use the following formula:
$°F = 9/5(K) - 459.67$

Sea level: In this report "sea level" refers to the National Geodetic Vertical Datum of 1929 (NGVD of 1929)—a geodetic datum derived from a general adjustment of the first-order level nets of both the United States and Canada, formerly called Sea Level Datum of 1929.

ADDITIONAL ABBREVIATIONS

DLS	detailed line survey
DOE	Department of Energy
DTN	data tracking number
ESF	Exploratory Studies Facility
GDF	Ghost Dance Fault
GTB	geothermal borehole
MF	major fault
NAD	northern access drift
NDR	northern drill room
NGDFA	Northern Ghost Dance Fault Alcove
PDB	Pee Dee Belemnite Formation of North Carolina
pmc	percent modern carbon
ppm	parts per million
TU	tritium units
Tptpmn	Tertiary Paintbrush Topopah Spring crystal-poor middle nonlithophysal
USGS	U.S. Geological Survey
YMP	Yucca Mountain Project

Results from Geothermal Logging, Air and Core-Water Chemistry Sampling, Air-Injection Testing, and Tracer Testing in the Northern Ghost Dance Fault, Yucca Mountain, Nevada, November 1996 to August 1998

By Gary D. LeCain, Lawrence O. Anna, *and* Michael F. Fahy

Abstract

Geothermal logging, air and core-water chemistry sampling, air-injection testing, and tracer testing were done in the northern Ghost Dance Fault at Yucca Mountain, Nevada, from November 1996 to August 1998. The study was done by the U.S. Geological Survey, in cooperation with the U.S. Department of Energy. The fault-testing drill room and test boreholes were located in the crystal-poor, middle nonlithophysal zone of the Topopah Spring Tuff, a tuff deposit of Miocene age. The drill room is located off the Yucca Mountain underground Exploratory Studies Facility at about 230 meters below ground surface. Borehole geothermal logging identified a temperature decrease of 0.1 degree Celsius near the Ghost Dance Fault. The temperature decrease could indicate movement of cooler air or water, or both, down the fault, or it may be due to drilling-induced evaporative or adiabatic cooling. In-situ pneumatic pressure monitoring indicated that barometric pressure changes were transmitted from the ground surface to depth through the Ghost Dance Fault. Values of carbon dioxide and delta carbon-13 from gas samples indicated that air from the underground drill room had penetrated the tuff, supporting the concept of a well-developed fracture system. Uncorrected carbon-14-age estimates from gas samples ranged from 2,400 to 4,500 years. Tritium levels in borehole core water indicated that the fault may have been a conduit for the transport of water from the ground surface to depth during the last 100 years.

Cross-borehole air-injection testing identified three zones that had different permeability and porosity values. The three zones corresponded to the structural units: footwall, fault zone, and hanging wall. The fault zone is a high-permeability zone associated with the main trace of the Ghost Dance Fault. Type-curve analysis indicated that the arithmetic mean of permeability values and of porosity values from the three structural units are: footwall 8.7×10^{-12} meter squared, and 0.04; fault zone 18.1×10^{-12} meter squared, and 0.13; hanging wall 5.0×10^{-12} meter squared, and 0.04. The three individual zones were homogeneous and isotropic. Numerical analysis using the U.S. Geological Survey AIR3D computer code indicated that the permeability and porosity values were: footwall 10.0×10^{-12} meter squared, and 0.07; fault zone 20.0×10^{-12} meter squared, and 0.20; hanging wall 5.0×10^{-12} meter squared, and 0.05. Analysis using a discrete-feature-network model successfully matched the pressure responses from the tests in the footwall and in the hanging wall but not in the fault zone. The discrete-feature-network model replicated the fracture networks and permeability in the footwall and hanging wall, but the fault zone was too broken to be analyzed using a discrete-feature model. Results from the discrete-feature model

indicated that it may be possible to increase the scale of the discrete-feature simulations to predict pressure responses at larger dimensions for areas that have fracture networks similar to the fracture networks in the footwall and hanging wall of the Ghost Dance Fault.

Cross-hole convergent-tracer tests had advective traveltimes that ranged from 0.011 to 1.110 days. Longitudinal-dispersivity values ranged from 0.06 to 2.63 meters. Tracer tests done in the footwall of the Ghost Dance Fault had transport-porosity values that ranged from 0.003 to 0.032 and had an average of 0.013. Tracer tests done in the fault zone had transport-porosity values that ranged from 0.004 to 0.034 and had an average of 0.014. Tracer tests done in the hanging wall had transport-porosity values that ranged from 0.001 to 0.070 and had an average of 0.013. The wide range in transport-porosity values may indicate that the test scale was smaller than the representative elementary volume. The tracer tests did not identify any directional control; slow and fast tracer-transport pathways occur in the same direction and plunge. Particle tracking using the discrete-feature model identified flow paths that were as much as six times longer than the linear distance. The long flow paths are a partial explanation of the large transport-porosity values. Results from the discrete-feature model indicated that it may be possible to increase the scale of the discrete-feature simulations to predict traveltimes at larger dimensions for areas that have fracture networks similar to the footwall and hanging wall of the Ghost Dance Fault.

INTRODUCTION

The Yucca Mountain Project (YMP) is a scientific study by the U.S. Department of Energy (DOE) to evaluate the potential for geologic disposal of high-level radioactive waste in an unsaturated-zone desert environment. The potential repository site at Yucca Mountain is located approximately 130 kilometers (km) northwest of Las Vegas, Nevada, near the DOE Nevada Test Site (fig. 1). The U.S. Geological Survey (USGS) has been conducting geologic and hydrologic studies of the potential repository site for the DOE. These studies are to quantify the geologic and hydrologic characteristics of Yucca Mountain and to conceptualize and model gas and liquid flow at the potential repository site.

Geothermal logging, air and core-water chemistry sampling, air-injection testing, and tracer testing were done at Yucca Mountain in the northern Ghost Dance Fault (GDF). The GDF was accessed through the Northern Ghost Dance Fault Alcove (NGDFA) that was constructed off the Yucca Mountain underground Exploratory Studies Facility (ESF). The goals of the fault testing were to quantify the permeability values, porosity values, tracer-transport characteristics (transport porosity and longitudinal dispersivity), and fluid ages of water in the GDF and the volcanic rocks (tuff) of the footwall and the hanging wall. The permeability, porosity, and tracer-transport characteristics of these tuffs control the movement of fluids in Yucca Mountain. Study of these parameters provides a conceptual understanding of local fluid flow in the unsaturated zone at Yucca Mountain. Quantified values of these parameters can be used in numerical modeling of the unsaturated zone to estimate fluid flux and transport through the mountain. Potential fluid movement in Yucca Mountain includes the transmission of water from the surface to the potential repository horizon, and below the horizon, and the transmission of gases from the potential repository horizon to the ground surface. Knowledge of the spatial and directional variability of the permeability and tracer-transport characteristics of the GDF is needed to formulate conceptual models and is needed as input to flow and transport models that attempt to represent the flow system at Yucca Mountain. This report presents the results from geothermal logging, gas and core-water chemistry sampling, air-injection testing, and tracer testing done in the NGDFA from November 1996 through August 1998. The location of the NGDFA and its relation to the potential repository are shown in figure 2.

Data presented in this report are classified as quality assured and non-quality assured. The quality-assured designation indicates that the data were collected following a YMP-approved quality-assurance program. The non-quality assured designation does not reflect on the accuracy or validity of the data but does indicate that the data may not have been

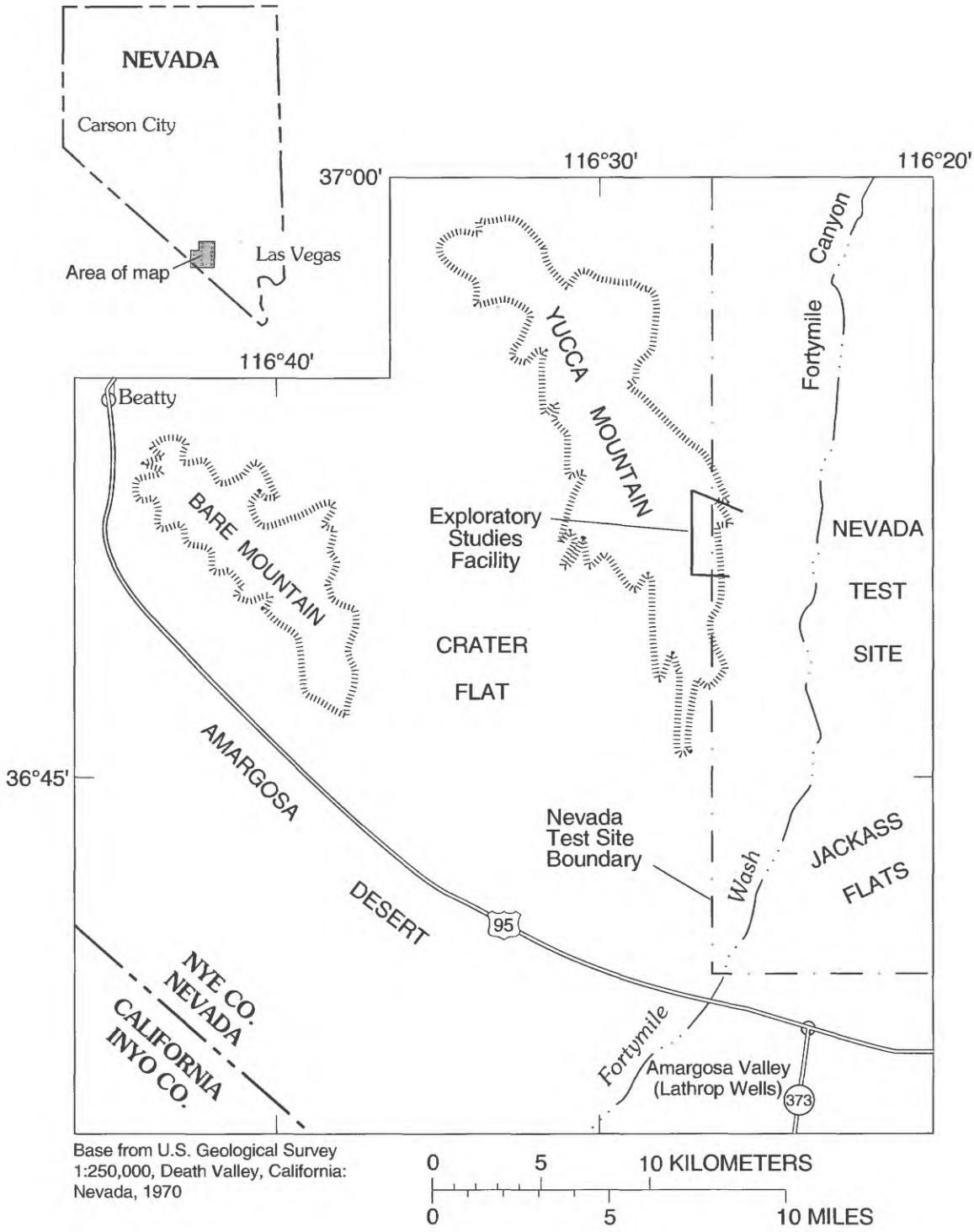

Figure 1. Location of the Nevada Test Site and the Exploratory Studies Facility at Yucca Mountain.

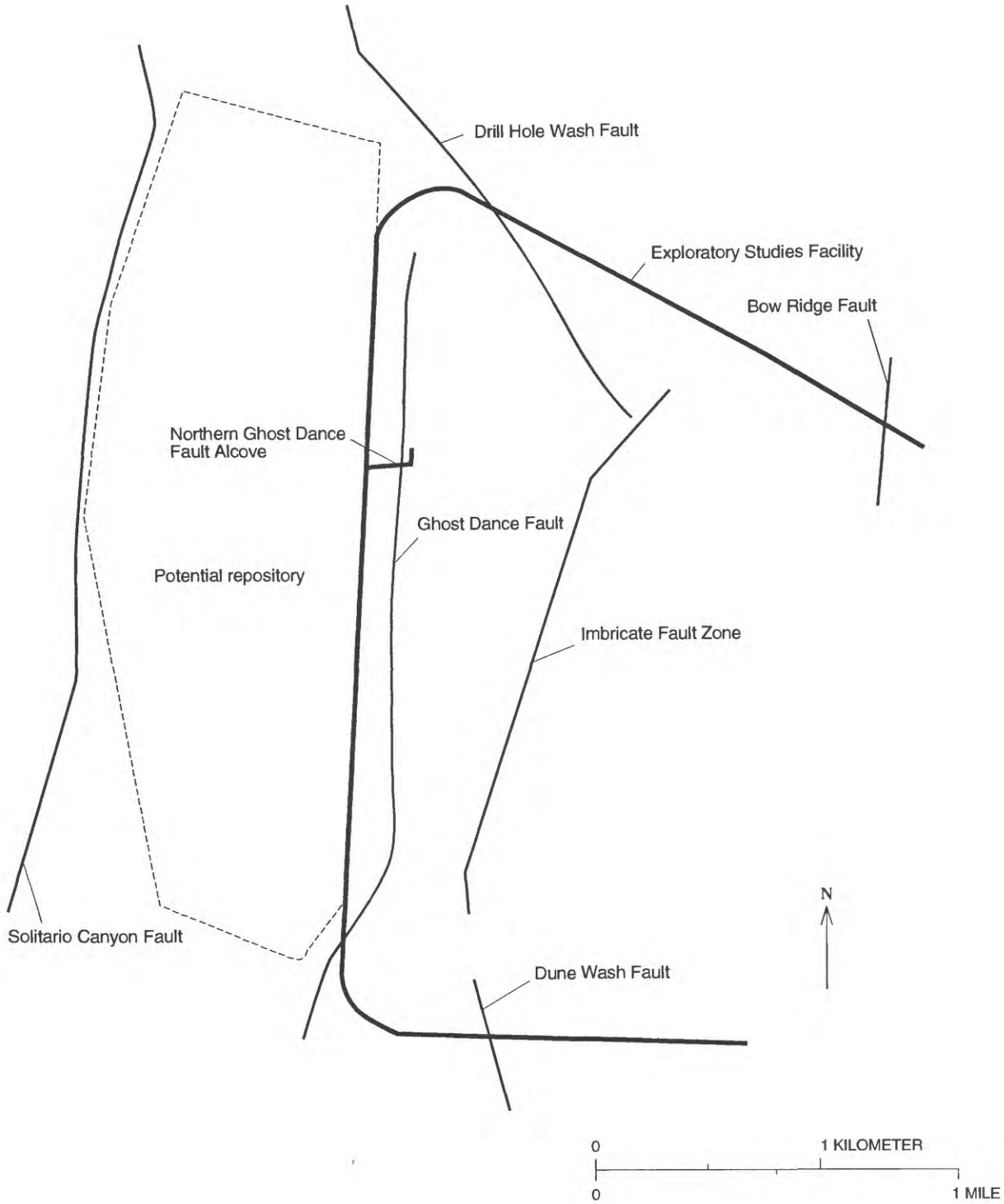

Figure 2. Location of the Ghost Dance Fault, Northern Ghost Dance Fault Alcove, and potential repository at Yucca Mountain.

collected under a YMP-approved quality-assurance program. As a part of the YMP quality-assurance program the data presented in this report are identified by data tracking numbers (DTN). A summary of the data, the DTNs, and the data quality-assurance status are included at the end of this report. All data presented in this report, with the exception of the tritium data, are classified as quality assured.

NORTHERN GHOST DANCE FAULT ALCOVE AND BOREHOLE CONSTRUCTION

The NGDFA was constructed in the YMP ESF during the second half of 1996 and the first half of 1997. The NGDFA consists of two sections—the northern GDF Access Drift (NAD), which provided access to the northern GDF Drill Room (NDR), which in turn provided a drilling and test room where test boreholes could be drilled into the fault (fig. 3). The NAD is located 3,737 m into the ESF (measured from the north entrance) and is about 230 m below the ground surface. The NAD and the NDR were excavated using a continuous miner. The NAD was initially constructed at a heading of due east (fig. 3) to a depth of 105 m (measured from the ESF centerline). From the face of the NAD, borehole NAD-GTB#1a was drilled horizontally, at a heading of due east, to a depth of 60 m and penetrated the GDF at a depth of about 49 m. A downhole video log was run on November 1, 1996, and a geothermal log on November 7, 1996. After the geothermal logging was completed, excavation of the NAD continued to a depth of 134.4 m, eliminating the upper 29.4 m of borehole NAD-GTB#1a. Geothermal logging,

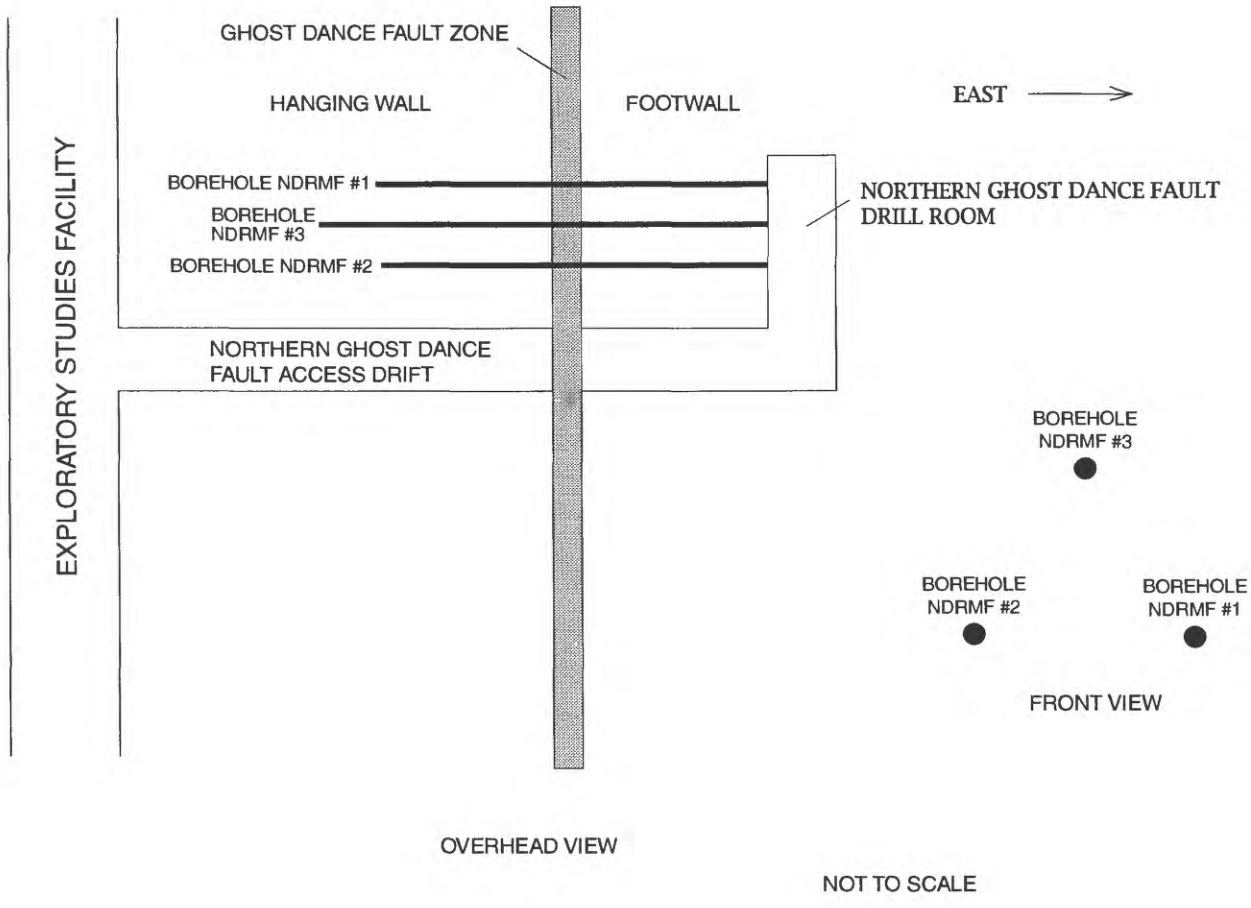

Figure 3. Northern Ghost Dance Fault Alcove and test boreholes.

hydrochemistry sampling, and air-injection testing were done in the remaining section of the borehole. After the testing was completed, construction of the NAD continued to a depth of 174 m. The NAD intersected the GDF at a depth of 152.1 to 152.7 m.

Following construction of the NAD and the NDR (May 1997), three horizontal boreholes were drilled from the NDR into the GDF. The boreholes were parallel and in a triangular configuration (fig. 3). The boreholes were dry-drilled and cored. A tracer gas of 1.0 part per million (ppm) sulfur hexafluoride (SF_6) was added to the drilling air. The borehole diameter was 10 cm and the core diameter was 6.2 cm. The locations, elevations, inclinations, bearings, and depths of the three Major Faults (MF) boreholes are listed in table 1.

Boreholes MF#1 and MF#2 were drilled in May and June 1997. Borehole MF#3 was drilled in October 1997. Following the completion of each borehole, downhole video and caliper logs were run.

Table 1. Locations, elevations, inclinations, bearings, and depths of the Exploratory Studies Facility Northern Drill Room Major Faults Boreholes #1, #2, and #3

Borehole	Elevation (meters)	Inclination	Bearing	Depth (meters)
MF#1	1,072.0	+00°39'58"	N271°14' 08"	30.5
MF#2	1,072.0	+00°27'44"	N270°49' 41"	30.6
MF#3	1,075.3	+01°42'07"	N271°29' 02"	34.4

GEOLOGY OF THE NORTHERN GHOST DANCE FAULT ALCOVE

The NGDFA and the MF boreholes are located in the crystal-poor, middle nonlithophysal zone, Topopah Spring Tuff (Tptpmn) of Miocene age. Borehole NAD-GTB#1a was drilled from the hanging wall of the GDF through the fault and into the footwall. The initial geologic interpretations of the fault and the broken zone (interval of intense fracturing) were based on video and caliper logs from borehole NAD-GTB#1a (DTN: LARO831422AQ97.001). The video logs identified the fault location at about 154 m from the ESF and identified a 12-m-wide broken zone. The 12-m-wide broken zone extended from 143 to 155 m, was variably brecciated, and consisted of fractured rock that had matrix- and clast-supported breccia zones. Following NAD excavation through the fault, geologic mapping identified the GDF as being located between stations 152.1 and 152.7 m on the right wall at spring line. The exposed brecciated zone is a 0.6- to 1-m-thick, matrix-supported, uncemented fault breccia that is derived from the wall rock. The footwall is intensely fractured from 152.7 m to 153.7 m and is slightly fractured from 153.7 m to 157.7 m. The hanging wall is moderately to intensely fractured from 142.1 m to the fault at 152.1 m. Distinct planes along the hanging wall and the footwall were not evident, and no slickensides were visible. The GDF is a normal fault with a strike/dip of 180/80 on the footwall and 175/82 on the hanging wall. The fault offset is approximately 3 m. The fault breccia is 60 percent matrix that consists primarily of clay- to sand-size particles and 40 percent rotated clasts that are angular to subangular and are as much as 20 cm in size. Average clast size is about 5 cm, and clasts are derived from the wall rock. No secondary calcite or silica/opal was visible in the breccia or surrounding rock (G.L.W. Eatman and others, Bureau of Reclamation, written commun., 1997, p. 168).

The three boreholes (MF#1, MF#2, and MF#3) intersected the GDF at depths of 13.6, 13.9, and 12.7 m, respectively. Downhole video and caliper logs identified an intensely fractured zone that extended from the main trace of the GDF about 1 m into the footwall and 3 m into the hanging wall. The intensely fractured zone is herein referred to as the "fault zone." Drilling logs (DTN:LARO831422AQ97.002) describe the footwall core samples as an ash-flow tuff that is densely welded, devitrified, and pale red; has minor pumice that is light gray to pale red; and that contains rare felsic and mafic lithic fragments that are 10 by 20 millimeters (mm) thick. The hanging wall is described as an ash-flow tuff that is grayish-orange pink; has 5 percent or less pumice that is very light gray, moderately flattened, and generally 10 mm or less in size; and has rare lithic fragments that are pale red to very light gray, angular to rounded, and are 2 to 5 mm in diameter. The footwall had a crushed appearance and tight anastomosing fractures of short length. The rock in the hanging wall is intact; pumice and lithic fragments are clearly visible. The fractures in the hanging wall are long and have various orientations. Many of the fractures in the hanging wall have measurable apertures (G.L.W. Eatman and others, Bureau of Reclamation, written commun., 1997).

TEST AND ANALYSIS METHODS

Field testing of the GDF was done from November 1996 to August 1998. The testing included: (1) video, caliper, and geothermal logging, (2) pneumatic monitoring, (3) gas and water chemistry sampling, (4) single and cross-hole air-injection testing, and (5) cross-hole tracer testing. The gas and water samples were analyzed for CO_2, $\delta^{13}C$, ^{14}C, and ^{3}H. Air-injection and tracer-test analysis included analytical and numerical methods.

Geothermal Logging in Borehole NAD-GTB#1a

Geothermal logging was done in borehole NAD-GTB#1a on November 7, 1996, and on December 3, 1996. The first geothermal log (November 7) was done when the borehole collar was located at 105 m from the ESF centerline and the borehole depth was 60 m. The second geothermal log was obtained on December 3 after the NAD had been extended to 134.4 m and the upper 29.4 m of the borehole had been excavated. The downhole-temperature logging tool consisted of a thermistor that had a very low thermal mass and was attached to a thin (approximately 100 μm) copper foil. The sensor was pressed against the borehole wall by a steel bowspring. The temperature resolution is approximately one millionth of a degree Celsius, and the temperature stabilization time is 1 second (John Sass, U.S. Geological Survey, oral commun., 1997). The first phase of logging was to insert the temperature logging tool to the bottom of the borehole and allow the tool to equilibrate for 5 to 10 minutes. Following equilibration, the temperature logging tool was withdrawn from the borehole and a continuous temperature profile was obtained. To limit heating caused by friction between the sensor and the borehole wall, the withdrawal speed was limited to 1 m per 3 minutes. This slow withdrawal limited the friction heating to 0.01°C or less.

Pneumatic Pressure Monitoring in Borehole NAD-GTB#1a

In-situ pneumatic pressures were monitored in borehole NAD-GTB#1a from December 19, 1996, to January 10, 1997. The downhole pneumatic pressures were monitored using a 30-m-long borehole liner and an uphole pressure transducer. The borehole liner is a flexible tube, 0.1 m in diameter, that is inverted into the borehole using internal pressure. The borehole liner contains 10 access ports that are connected to the uphole borehole collar by small-diameter nylon tubes. A schematic of the liner, access ports, and tubes is shown in figure 4. Once installed into the borehole, the internal pressure of the liner is maintained at 3.4 to 6.9 kPa. The internal pressure forces the liner against the borehole wall, isolating the borehole and creating monitor intervals of about 0.25 m in length that are separated from each other by from 1.5 to 3.0 m. Each isolated downhole-monitor interval contains an access port that was connected to a nylon tube that extended from the access port up the boreholes to the NDR. The nylon-access-port tubes were then connected to a solenoid valve and pressure transducer, and the pneumatic pressures in the isolated downhole-monitor intervals were recorded by a data logger.

Chemical Sampling in Borehole NAD-GTB#1a

Gas-phase chemistry samples were collected in borehole NAD-GTB#1a from December 4, 1996, to January 14, 1997, using the borehole liner (fig. 4). To obtain gas samples, the nylon-access-port tubes were connected to peristaltic pumps, and gas samples were pumped from the isolated downhole-monitor intervals. Gas samples for carbon-14 analysis were collected in molecular sieves. Gas samples for delta carbon-13 analysis were collected in mylar balloons. Before the gas sampling, the monitor intervals were pumped to evacuate any atmospheric and drilling-injected air. Carbon dioxide (CO_2) and SF_6 (used as a drilling-air tracer) were monitored using a gas chromatograph throughout the pumping period to assess the removal of the atmospheric and drilling-injected air and to determine when the gas sample represented that of rock gas. Stable CO_2 concentrations at levels substantially higher than atmospheric air (350 ppm) or alcove air (450 ppm) indicated that the gas being pumped from the borehole was rock gas. Low SF_6 concentrations (on the order of 0.01 ppm) also indicated that the drilling air had been successfully removed from the isolated downhole-monitor intervals. Water samples for tritium analysis were obtained from core from the borehole by using a vacuum distillation system. Most

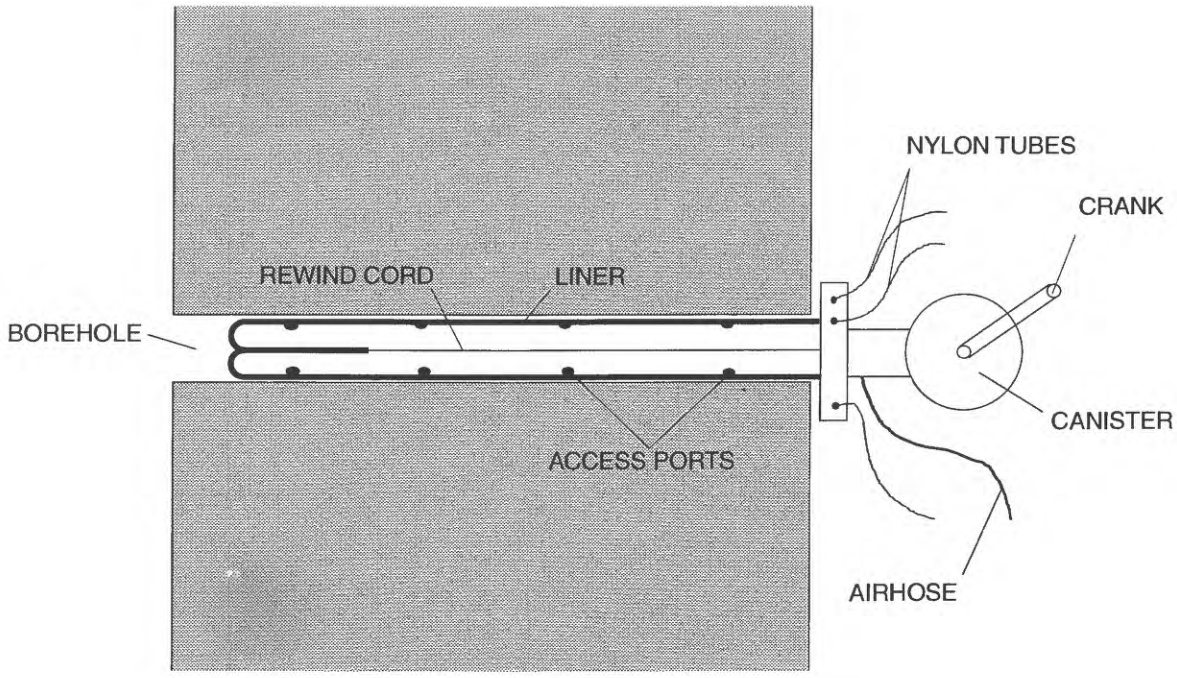

Figure 4. Borehole liner, access ports, and support equipment.

of the tritium analyses were done by the USGS in Denver, Colorado, and a few samples were sent to the University of Miami, Florida. The USGS used a liquid scintillation counter. The University of Miami used enriched samples and a gas-proportional counter; therefore, the Miami results had smaller standard deviations.

Chemical Sampling in the Northern Drill Room Boreholes

Gas-phase chemistry samples were collected in boreholes MF#1 and MF#2 from August 4 to August 20, 1998, using the borehole liner (fig. 4). The gas sampling and analysis were identical to those done in borehole NAD-GTB#1a. Water samples for tritium analysis were obtained from core from borehole MF#1 and analyzed at the University of Miami.

Single-Hole Air-Injection Testing and Analysis in Borehole NAD-GTB#1a

Single-hole air-injection testing was done in borehole NAD-GTB#1a from January 15 to February 23, 1997. A schematic of a single-hole air-injection testing system is shown in figure 5. The field equipment consisted of the downhole-packer system, the air-injection system, and the data-acquisition system. Test intervals were selected from a review of the borehole video logs. Following the selection of a test interval, two pneumatic packers were inserted into the borehole and straddled the selected test interval. The packers then were inflated, using compressed air, isolating the test interval. After the packers were inflated and the pressure in the test interval had stabilized, compressed air was injected into the isolated test interval through a nylon tube that connected the test interval to an uphole air compressor. Sulfur hexafluoride was added to the injection air as a tracer (10.0 ppm), and the air-injection rate was controlled and monitored by mass-flow controllers. The absolute pressure and temperature in the test interval were monitored by a pressure transducer and a thermistor mounted between the downhole packers. All data were recorded on a data logger. The pressure responses measured in the test intervals usually showed an initial pressure increase followed by a period of decreasing pressure. The period of decreasing pressure was due to water redistribution (LeCain, 1998). Air injection was continued until the test-interval pressure neared steady state—approximately 10 minutes. Twelve of the 13 test intervals had lengths of 1 m; one test interval had a length of 12 m.

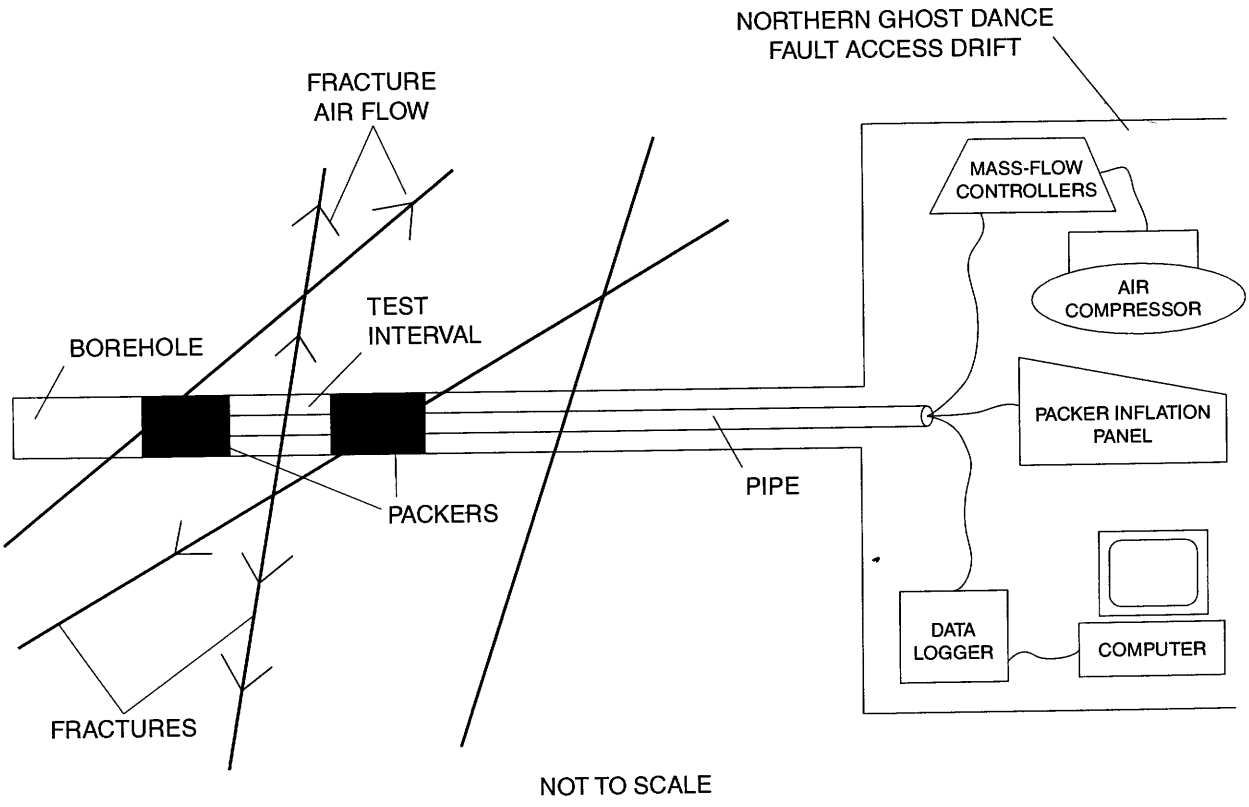

Figure 5. Single-hole air-injection testing system.

Initial permeability values were calculated for each test using a modified version of the Hvorslev (1951, p. 31, case 8) steady-state solution. The solution is for elliptical flow when the length of the injection interval is substantially greater than the radius of the injection interval. The analysis was developed to evaluate flow in an equivalent porous medium (gravel and alluvium). Application of the method to fractured tuff assumes that the fracture-flow system is sufficiently connected and extensive so that the fractured tuff could be treated as an equivalent porous medium. The full derivation of equation 1 is presented in LeCain (1997, p. 6 and 7).

$$k = \frac{P_{sc}\ Q_{sc}\ \mu\ ln\left(\frac{L}{2r_w} + \sqrt{1+\left(\frac{L}{2r_w}\right)^2}\right)\ T}{\pi\ L\ (P_{ss}^2 - P_0^2)\ T_{sc}} \quad (1)$$

where

k = permeability, in meters squared;

P_{sc} = standard pressure, in pascals;

Q_{sc} = flow rate at standard conditions, in cubic meters per second;

μ = dynamic viscosity, in pascal seconds;

L = injection-interval length, in meters;

r_w = borehole radius, in meters;

T = injection air temperature, in kelvin;

P_{ss} = pressure at steady state, in pascals;

P_0 = pressure at time zero, in pascals; and

T_{sc} = temperature at standard conditions, in kelvin.

To evaluate turbulence, multiple tests at variable flow rates were done on each test interval. Air-injection rates ranged from 10 to 800 standard liters per minute (sLpm). A more detailed examination of turbulence in air-injection testing in fractured rock is available in LeCain (1998). Ramey (1982) developed the generalized equation,

$$H_w = BQ + CQ^n\ , \quad (2)$$

where

H_w = drawdown, in meters;
B = formation-loss term, in seconds per meter squared;
Q = flow rate, in cubic meters;
C = well-loss term, units dependent on exponent n; and
n = exponent less than 2.

The first term on the right of equation 2 represents laminar flow conditions where Darcy's law is valid. The second term represents non-Darcian flow due to turbulence in the borehole or in the fractures. The drawdown during Darcian (laminar) flow can be represented by the first term only. During non-Darcian flow, the second term needs to be included. Air-injection testing in fractured rock generally involves a combination of laminar and turbulent fracture flow.

Equation 2 was modified for air-injection testing by substitution of $(P_{ss}^2 - P_0^2)$ for drawdown, and both sides of the equation were divided by the flow rate (Q_{sc}) to yield equation 3,

$$\frac{(P_{ss}^2 - P_0^2)}{Q_{sc}} = CQ_{sc}^{n-1} + B \qquad (3)$$

where
P_{ss}^2 = steady-state pressure squared, in pascals squared; and
P_0^2 = pressure squared at time zero, in pascals squared.

Assuming that $n = 2.0$, equation 3 indicates that an arithmetic plot of the steady-state $(P_{ss}^2 - P_0^2)/Q_{sc}$ values, from multiple flow-rate tests, on the y-axis and the Q_{sc} values on the x-axis gives a y-intercept equal to B when Q_{sc} is zero. As Q approaches zero, Darcy's law is valid; that is, there are no turbulent or inertial effects. Equations 1 and 3 can then be combined in equation 4 to provide a laminar-flow air-injection permeability value that is based on the zero-flow intercept B.

$$k = \frac{P_{sc}\ \mu\ \ln\left(\frac{L}{r_w} + \sqrt{1 + \left(\frac{L}{2r_w}\right)^2}\right)}{\mu\ L\ B\ T_{sc}}\ T \qquad (4)$$

Non-Darcian flow was identified as a decrease in the calculated permeability values with increasing flow rates. A check was done by preparing arithmetic and log-log plots that had the air-injection pressure squared differences $(P_{ss}^2 - P_0^2)$ on the y-axis and the flow rate (Q) on the x-axis. Darcian (laminar) flow $(H_w = BQ)$ was indicated by a linear arithmetic plot and a log-log plot with a slope of one. A nonlinear arithmetic plot and a log-log plot that had a slope greater than one indicated non-Darcian flow. A slope of zero would indicate laminar flow, and a positive slope would indicate turbulence. The plot was extrapolated to the y intercept, and the intercept was used in equation 4 to calculate the fractured-rock permeability values presented in this report.

Cross-Hole Air-Injection Testing and Analysis in the Northern Drill Room Boreholes

Test Methods

Cross-hole air-injection tests were done between the three NDR boreholes in three phases from August 1997 to June 1998. Cross-hole testing consisted of injecting air into an isolated interval of a borehole (injection borehole) and monitoring the pressure response in isolated monitor intervals in other boreholes (monitor boreholes). The first phase of testing was done following the construction of boreholes MF#1 and MF#2; the testing consisted of 11 tests using borehole MF#1 as the monitor borehole and borehole MF#2 as the injection borehole. Following the construction of borehole MF#3, the second phase of testing was done; testing consisted of 13 tests using boreholes MF#1 and MF#2 as monitor boreholes and borehole MF#3 as the injection borehole. The third phase of testing consisted of 13 tests using boreholes MF#2 and MF#3 as monitor boreholes and borehole MF#1 as the injection borehole. The injection borehole was instrumented with the same dual-packer gas-injection system used in the single-hole air-injection testing. The monitor boreholes were each fitted with 10 packers that separated each monitor borehole into 10 pressure-monitor intervals. A schematic of the NDR cross-hole air-injection testing system is shown in figure 6. The packer lengths for the monitor boreholes ranged from 1.0 to 8.0 m, and the monitor-interval lengths ranged from 0.6 to 4.0 m. Each packer was connected to an uphole packer-inflation panel by a 0.5-mm high-pressure-nylon inflation tube. The packer-inflation panel was

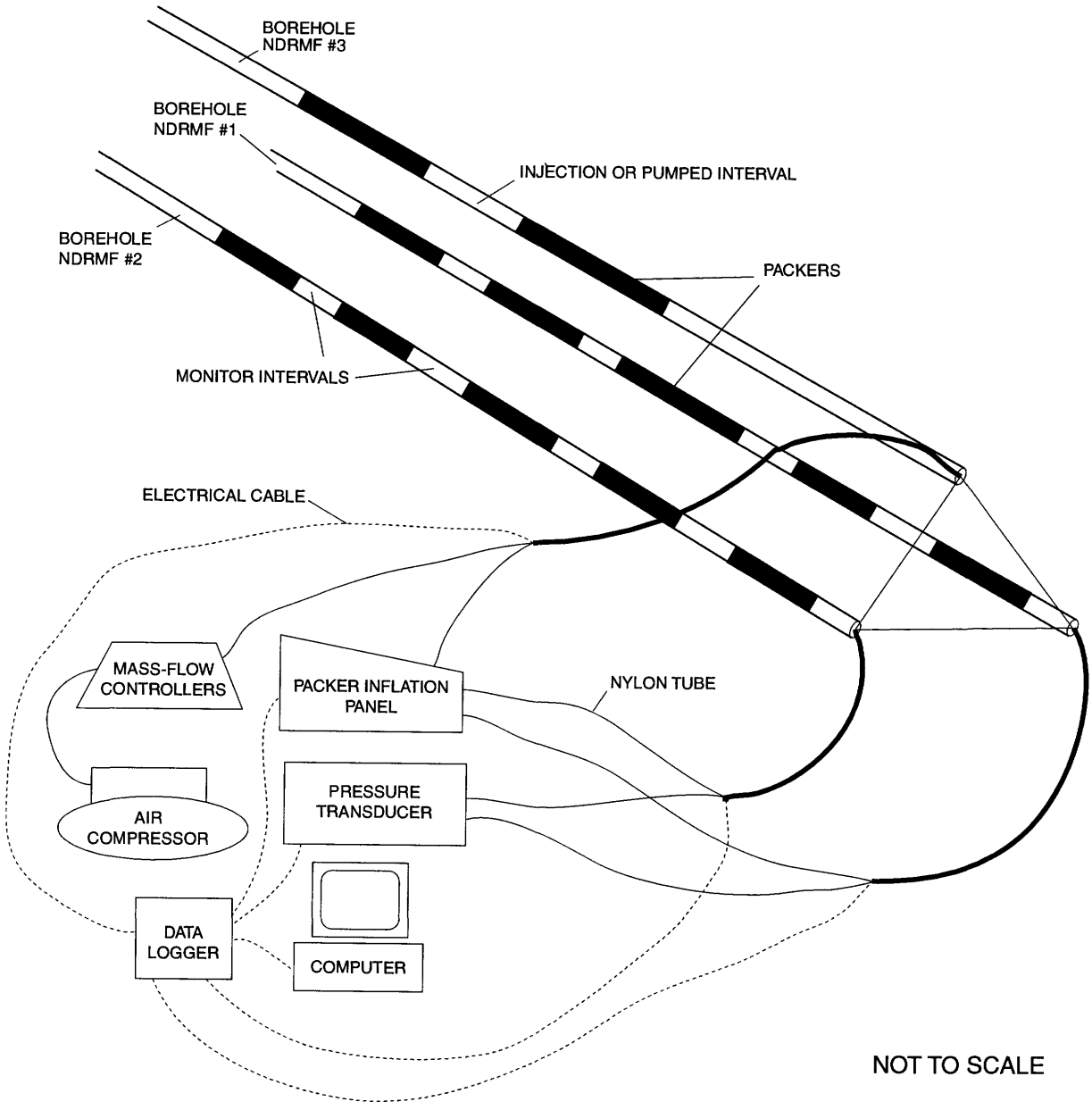

Figure 6. Cross-hole air-injection testing system.

used to inflate the packers and to monitor the individual packer-inflation pressures. Each monitor interval was connected to an uphole pressure-transducer panel by a 1.0-mm nylon tube. Each monitor-interval tube had a dedicated pressure transducer that measured the absolute pressure in the monitor intervals. In addition, the tubes could be disconnected from the pressure transducers and used for gas sampling or tracer-gas injection. The air-injection rate for the cross-hole testing was 500 sLpm and was monitored and controlled by mass-flow controllers. Air was injected until the pressure in the injection interval and in the monitor intervals neared steady state, about 3 hours.

Analysis Using Type Curves

Type-curve analysis included an initial examination of the shape and the steady-state values of the

pressure responses in the injection and the monitor intervals. The pressure responses were examined to identify any patterns that would indicate any effects of direction or location on the permeability and porosity of the fractured tuff. The initial examination included composite log-log plots that were normalized by plotting the monitor-interval pressure squared differences times the radial flow distance on the y-axis and time divided by the radial flow distance squared on the x-axis. If the medium is homogeneous and isotropic, the normalized data plots will form a single curve. Following the initial examination, type-curve matching was used to analyze the pressure responses of the monitor intervals. The analysis of tests done in the hanging wall and the footwall assumed a spherical flow geometry and used the complementary error function to estimate permeability and porosity values. The analysis was developed to evaluate flow in an equivalent porous medium; therefore, application of the method to fractured tuff assumes that the fracture-flow system is sufficiently connected and extensive so that the fractured tuff could be treated as an equivalent porous medium. The full solution is presented in LeCain (1995, p. 12). The analysis assumed that the injection and the monitor intervals could be represented as points in a large homogeneous and isotropic system. The solution defines the change in dimensionless pressure as,

$$\Delta P_D = \frac{1}{2} erfc \left(\frac{r_D^2}{4t_D} \right)^{\frac{1}{2}} , \quad (5)$$

where

$$\Delta P_D = \frac{(P^2 - P_i^2)}{P_i^2 \, q_D} , \quad (6)$$

$$r_D = \frac{r}{r_w} , \quad (7)$$

$$t_D = \frac{kt}{\phi \mu \bar{c} r_w^2} , \quad (8)$$

$$q_D = \frac{P_{sc} Z T q_{sc} \mu}{\pi k r P_i^2 \, T_{sc}} , \quad (9)$$

where

erfc = complementary error function;
P_D = dimensionless pressure;
P = pressure, in pascals;
P_i = initial pressure, in pascals;
r_D = dimensionless radius;
r_w = well radius, in meters;
r = radius, in meters;
t_D = dimensionless time;
k = permeability, in square meters;
t = time, in seconds;
ϕ = porosity, in cubic meters per cubic meter;
μ = gas dynamic viscosity, in pascal seconds;
$\bar{c}$ = average gas compressibility, in pascal^{-1}.
q_D = dimensionless flow;
P_{sc} = pressure at standard conditions, in pascals;
Z = gas constant (assumed to be 1.0), dimensionless;
T = temperature, in kelvin;
q_{sc} = gas flow at standard conditions, in cubic meters per second; and
T_{sc} = temperature at standard conditions, in kelvin.

A log-log plot of the pressure-squared differences on the y-axis and time on the x-axis (t = 0 at start of the injection test) was overlaid on the type curve defined by equation 5 and a match point was selected. By using the match point variables, the permeability value is

$$k = \frac{T Q_{sc} \mu P_{sc} \Delta P_D}{(P^2 - P_i^2) \; r \; \pi T_{sc}} , \quad (10)$$

and porosity is calculated by

$$\phi = \frac{k t \bar{c}}{\frac{t_D}{r_D^2} \mu r^2} . \quad (11)$$

Analysis of the tests done in the fault zone assumed a radial flow geometry and used a modified version of the Theis (1935) exponential integral function to estimate the permeability and porosity values.

The solution defines the change, in dimensionless pressure (Earlougher, 1977, p. 192) as

$$\Delta P_D = -\frac{1}{2} Ei\left(-\frac{r_D^2}{4t_D}\right), \quad (12)$$

where

Ei = exponential integral function.

The parameters used in equation 12 are identical to those defined for equation 5 except for,

$$q_D = \frac{P_{sc} Z T q_{sc} \mu}{\pi k h P_i^2 T_{sc}} \quad (13)$$

where

h = length of the injection interval, in meters.

A log-log plot of the pressure squared differences on the y-axis and time on the x-axis (t = 0 at start of the injection test) was overlain on the type curve and a match point was selected. By using the match point variables, the permeability value is

$$k = \frac{T Q_{sc} \mu P_{sc} \Delta P_D}{\Delta P^2 h \ \pi T_{sc}} . \quad (14)$$

Porosity is calculated by using the same equation that was used in the spherical flow solution, equation 11.

Numerical Analysis Using AIR3D

Following the type-curve analysis, a numerical model of the northern GDF flow system was developed using the USGS finite-difference model AIR3D (Joss and Baehr, 1995). Computer code AIR3D adapts the ground-water flow simulator MODFLOW (McDonald and Harbaugh, 1988) for use with three-dimensional air flow in unsaturated flow systems. A finite-difference numerical model of the footwall, fault zone, and hanging wall was developed. The numerical model was based on the geological interpretations of the NAD and the NDR (G.L.W. Eatman and others, Bureau of Reclamation, written commun., 1997); the borehole video logs; and personal inspection of the NAD footwall, fault zone, and hanging wall. The model used an equivalent continuum approach that had a grid of 40 layers, 25 columns, and 25 rows. The model layers had a constant 2-m dimension, whereas the column and row dimensions ranged from 0.1 m at the center of the grid to as much as 10 m at the boundaries. The dimensions were selected to ensure boundary effects would not affect the simulation results. The model assumed a heterogeneous flow system that had three homogeneous-isotropic zones. The three zones corresponded to the footwall, fault zone, and hanging wall. The model was scaled, and the grid nodes were identified that matched the air-injection and monitor intervals in order to replicate the three-dimensional cross-hole air-injection field testing. The model was run using air-injection grid nodes and mass-flow rates that replicated selected field tests. At the completion of the model run, plots of the grid-node pressure responses, which represented monitor intervals, were visually compared to the field-test pressure responses. By using these comparisons, the simulated permeability and porosity values were adjusted, and the model was rerun. The rerun pressure responses again were compared to the field pressure responses. This iterative process was repeated using different permeability and porosity values, different air-injection grid nodes, and different monitor-interval grid nodes until a satisfactory match between the simulated pressure responses and the field pressure responses were obtained.

Discrete-Feature Analysis Using FRACMAN

Following the analytical and the numerical analysis, a discrete-feature network (DFN) model was developed using the computer code FRACMAN (Dershowitz and others, 1994). The objective of the DFN modeling was to develop a fracture-flow model that represents the GDF fracture system more accurately than the equivalent porous-medium models. A better understanding of the fracture-flow process may be valuable for predicting flow and transport at other locations and at different scales. The DFN analysis used the forward modeling approach of FRACMAN to develop a three-dimensional DFN model. The geometry and spatial distributions for the fracture systems in the model were based on the detailed line survey (DLS) fracture data from the NAD and NDR. The DLS fracture mapping mapped only fractures with trace lengths greater than 30 cm (DTN:

LARO970808314224.014). Fracture lengths ranged from 30 cm to 22 m.

The DLS fracture data were analyzed using CLUSTRAN fracture-analysis software and visual inspections of equal-area Schmidt plots. Fracture-distribution types and fracture amounts were defined for orientation, size, intensity, and dispersion. Fracture intensity was based on the scale-independent ratio of fracture area to rock volume. The fractures were classified into fracture sets based on their dip and strike. The fracture-set lengths were analyzed to determine a mean, standard deviation, and distribution type. The fracture data were used to estimate an effective fracture radius (or size) from the trace length distribution using the FRACMAN-FRACSYS module.

Fracture size is related to fracture area per rock volume and is a direct input parameter into the three-dimensional DFN model. The FRACSYS algorithm allows an initial estimate of the fracture size distribution and simulates a length distribution. The initial estimate was changed by optimization algorithms until the simulated length distribution matched the mapped length distribution from the DLS. The optimized estimate then was used as the fracture size distribution for the DFN model. This process was used to analyze each fracture subunit of the network. The process eliminates censoring and truncation bias. To minimize fracture-orientation bias, more than one orientation of tunnel segments was used; the orientations were normalized to the number of fractures and included into one orientation distribution pool. Mapped fault data were included exactly as mapped in the NAD and NDR. Physical features, such as boreholes and tunnels, were replicated to the scale and location of the measured field boundaries.

The DFN model was calibrated by the generation of 10 DFN simulated fracture systems based on the CLUSTRAN fracture data base. The fracture characteristics of the 10 simulated fracture systems then were compared to the DLS field data. When the simulated DLS number of fractures per meter was within one standard deviation of the field DLS, the fracture component of the DFN model was considered calibrated. Following the model calibration, transmissivity values for fractures were assigned to the fracture systems. The DFN transmissivity values were based on the results of the single-hole and the cross-hole air-injection testing. The single-hole and cross-hole tests from the field used pneumatic conditions; however, the FRACMAN modeling code simulated hydraulic conditions. As a result, pneumatic parameters of pressure and flow rates were converted to hydraulic parameters in the DFN model. The DFN model then simulated the cross-hole air-injection field tests. The simulated pressure responses then were compared to the field-measured pressure responses. This iterative process was repeated until the model results matched the field results, indicating that the geometric, hydraulic, and spatial properties were acceptable. Three cross-hole air-injection tests were simulated—tests 25, 32, and 36. The injection intervals of the three tests were located in borehole MF#1. The injection interval for test 25 was in the hanging wall, the injection interval for test 32 was in the fault zone, and the injection interval for test 36 was in the footwall. The monitor intervals were in boreholes MF#2 and MF#3 and were located throughout the footwall, the fault zone, and the hanging wall.

Cross-Hole Tracer Testing and Analysis in the Northern Drill Room Boreholes

Test Methods

Cross-hole convergent-tracer tests were done between intervals that had cross-hole pneumatic connections. Convergent-tracer testing used the same equipment as the cross-hole air-injection testing (fig. 6) except that the air compressor was replaced with a vacuum pump. The interval isolated by the dual-packer assembly was pumped at about 30 sLpm, creating a pneumatic gradient toward the pumped interval. When the flow system reached steady state, a slug of SF_6 (0.3 to 0.6 L of 10-percent SF_6) and a slug of helium (He) (0.3 to 0.6 L of 10-percent He) were released in monitor intervals in a different borehole. The tracers flowed along the pneumatic gradient to the pumped interval where the tracer concentrations were measured using a gas chromatograph for the SF_6 and a mass spectrometer for the He. The pumping rate was controlled by mass-flow controllers; the pneumatic gradient was monitored by pressure transducers. Tracer-release concentrations were selected so that the peak concentration at the pumped interval approached 35 ppm. Because the zone of decreased pressure around the pumped interval was small, limited by the pumping rate, the linear distances between the tracer release interval and the pumped interval were gener-

ally limited to less than 7 m. Twenty-one cross-hole tracer tests were done in three phases from November 1997 to June 1998. The three phases of convergent-tracer testing followed the three phases of the cross-hole air-injection testing. Tests 1 through 8 used borehole MF#2 as the pumped borehole, and isolated intervals in borehole MF#1 were used for tracer release. During tests 1 through 8, the He and the SF_6 tracers were released simultaneously in the same isolated interval in borehole MF#1. During tests 9 through 16, borehole MF#3 was the pumped borehole; the He tracer was released in isolated intervals in borehole MF#2, and the SF_6 tracer was released in isolated intervals in borehole MF#1. During tests 17 through 21, borehole MF#1 was the pumped borehole; the He tracer was released in isolated intervals in borehole MF#3, and the SF_6 tracer was released in isolated intervals in borehole MF#2.

Analysis Using Type Curves

The cross-hole tracer tests were analyzed using type curves (Moench, 1995). The method assumes that the fracture system can be treated as an equivalent porous medium and is based on mass conservation and Fick's law. Solute transport is described by the advection-dispersion equation. The details of this derivation are beyond the scope of this report but are given in Bear (1979, starting on p. 239). The solution was used with air and gas tracers and assumes that gas compression effects are minimal; this is a reasonable assumption because the tracer-test pressure gradients were less than 15.0 kPa (16.7 percent of atmosphere). The dual-porosity radial-flow analytical solution (Moench, 1995, p. 1824) was used to solve the porous-medium, advection-dispersion equation:

$$\frac{1}{r}\frac{\partial}{\partial r}\left(rD_L\frac{\partial C}{\partial r}\right) - v\frac{\partial C}{\partial r} = R\frac{\partial C}{\partial t} \qquad (15)$$

where

r= radial distance, in meters;
D_L= longitudinal pneumatic dispersion, in square meters per second;
C= tracer concentration, in kilograms per cubic meter;
v= velocity, in meters per second;
R= tracer retardation, dimensionless; and
t= time, in seconds.

Type curves were generated for a range of Peclet numbers using the analytical solution for radially-convergent flow for a single-porosity system. The single-porosity type curves are log-log plots of dimensionless concentration (C_d) as a function of dimensionless time (t_d) where:

$$C_d = \frac{C\pi h\phi_T\ (r^2 - r_w^2)}{M}, \qquad (16)$$

and

$$t_d = \frac{t}{t_a}, \qquad (17)$$

where

h= length of tracer release interval, in meters;
ϕ_T= transport porosity, in cubic meters per cubic meter;
r_w= well radius, in meters;
M= mass of released tracer, in kilograms;
t_a= advective travel time, in seconds.

The tracer test data were plotted as log-log plots of normalized concentration as a function of time:

$$\frac{C - C_b}{C_{max} - C_b}, \qquad (18)$$

where

C_b= background tracer concentration, in kilograms per cubic meter;
C_{max}= maximum pumped tracer concentration, in kilograms per cubic meter.

The rising portion of the data curves were matched to the type curves. Matching only the rising portion of the curves ignored the diffusion process because it was assumed that the effect of diffusion is minimal on the rising limb of the breakthrough curve. The normalized tracer curves and curve matching provided estimates of the advective traveltime (time to the center of mass) and the Peclet numbers.

The Peclet number is defined as

$$Pe = \frac{r}{\alpha} , \qquad (19)$$

where

α = longitudinal dispersivity, in meters.

The transport porosity was determined by

$$\phi_t = \frac{(q\ t_a)}{[\pi\ h(r^2 - r_w^2\ )]} \qquad (20)$$

where

q = gas pump rate, in cubic meter per second.

A limitation of the type-curve analysis was that the solution assumed an idealized radial-flow geometry while the field-flow geometry was a combination of spherical and leaky radial flow. To compensate for the nonideal flow geometry, the analysis assumed that the tracer release interval component (h) of equation 20 was a constant 8.0-m "effective length." The "effective length" was based on an estimated 8.0-m maximum zone of influence (measurable pressure drawdown) extending out from the pumped interval during tracer testing. Use of an "effective length" provided some compensation for the greater advective traveltimes caused by the nonradial flow components. The calculated transport porosity (sometimes called effective porosity) is a composite of the physical factors that influence the movement of the tracer from the release point to the pumped interval. These parameters include, but are not limited to, the fracture-flow path length, the number of fractures, the fracture-aperture distribution, the rugosity of the fracture walls, the tortuosity of the flow path, matrix interaction, and sorption. No attempts were made to estimate the diffusion coefficients because of the difficulty of defining an equivalent radius in a fracture-flow system that is nonuniform.

Discrete-Feature Analysis Using MAFIC

The MAFIC code (Miller and others, 1994), in combination with the DFN model developed in FRACMAN, was used to analyze the gas-tracer-transport tests. The MAFIC code uses the solute-transport equation in one dimension as described by Bear (1972, p. 617) and presented in equation 21.

$$\frac{\partial}{\partial_x}\left[(d_L \cdot V) + D\frac{\partial_c}{\partial_x}\right] - V\frac{\partial_c}{\partial_x} + C_s \cdot Q_s = \frac{\partial_c}{\partial_t} , \qquad (21)$$

where

V = Darcian velocity, in meters per second;
d_L = longitudinal dispersivity, in meters;
D = coefficient of molecular diffusion, in square meters per second;
x = length, in meters;
c = the solute concentration, in kilograms per cubic meter;
t = time, in seconds;
Q_S = external source, in seconds^{-1};
C_S = concentration of tracer at external source, in kilograms per cubic meter.

The solute transport was simulated using a particle-tracking method. The method represents the concentration of solutes in the solvent using a finite number of discrete particles of equal mass. Each particle represents a fraction of the total solute. Initial conditions imply that all particles are initially located in the fractures. At each time step, particles are moved according to a deterministic advective component and a stochastic dispersive component. Particles were introduced at a source (tracer-release interval) in the first 200 seconds of the simulation and were removed at a specified sink (pumped interval). Average concentrations and total particle mass were calculated at the end of each time step. The advective component was proportional and parallel to the velocity vector at the current particle location. The dispersive component was proportional to the square root of the advective component (Miller and others, 1994). Mass transfer between the matrix and fractures was ignored.

The DFN model simulation that best matched the cross-hole air-injection tests 25, 32, and 36 was used to model the tracer-transport field tests. Three tracer field tests were modeled: tracer-test number 17, where the pumped interval was in the hanging wall; tracer-test number 21, where the pumped interval was in the footwall; and tracer-test number 15, where the pumped interval was in the fault zone. For all tests, the sink (pumped intervals) was in borehole MF#3, and the source (tracer release intervals) was in MF#1 and MF#2.

TEST RESULTS

Caliper and video logging was successful in borehole NAD-GTB#1a and in boreholes NDR-MF#1, 2 and 3. The caliper and video logs were used to identify geologic features and to locate test intervals. Geothermal logging, pneumatic monitoring, gas and water chemistry sampling, and single-hole air-injection testing were successfully done in borehole NAD GTB#1a. Gas and water chemistry sampling, single and crosshole air-injection testing, and cross-hole gas-tracer testing were successfully done in the NDR boreholes.

Results from Geothermal Logging in Borehole NAD-GTB#1a

The geothermal logs from November 7 and December 3, 1996, from borehole NAD-GTB#1a (DTN: GS970383122410.005) are shown in figure 7. Both logs showed near-surface temperature gradients that indicated ventilation effects to depths of 3 to 5 m. The geothermal log from November 7, 1996, completed when the NAD face was at 105 m from the ESF centerline, identified a 0.1°C temperature decrease throughout the 38- to 50-m long, 12-m-wide broken zone (143 to 155 m from the ESF centerline) that had been identified in the video log. The temperature decrease could indicate movement of cool air, or water, or both, down the 12-m-wide broken zone. The barometric pressure was rising on November 6 and 7, 1996, and supports the concept of cool, shallow air moving down the 12-m-wide broken zone. The geothermal log from December 3, 1996, completed when the NAD face was at 134.4 m from the ESF centerline, did not show the previously recorded temperature drop in the 12-m broken zone but identified a 0.05°C temperature increase at or near the main trace of the fault (49 m in the borehole and 154 m from the ESF centerline). The barometric pressure was decreasing on December 2 and 3, 1996, which supports the concept of deep, warm air moving up the main trace of the GDF. The stabilization of the temperature in the 12-m-wide broken zone between November and December indicated that the November temperature drop may have been due to drilling-induced evaporative cooling or gas-expansion adiabatic cooling. Other temperature fluctuations may be due to drilling effects or, possibly, due to the variable borehole diameter. A more thorough understanding of the effect of barometric pressure on the temperature in the GDF and the 12-m-wide broken zone require geothermal logging during a range of barometric pressure fluctuations.

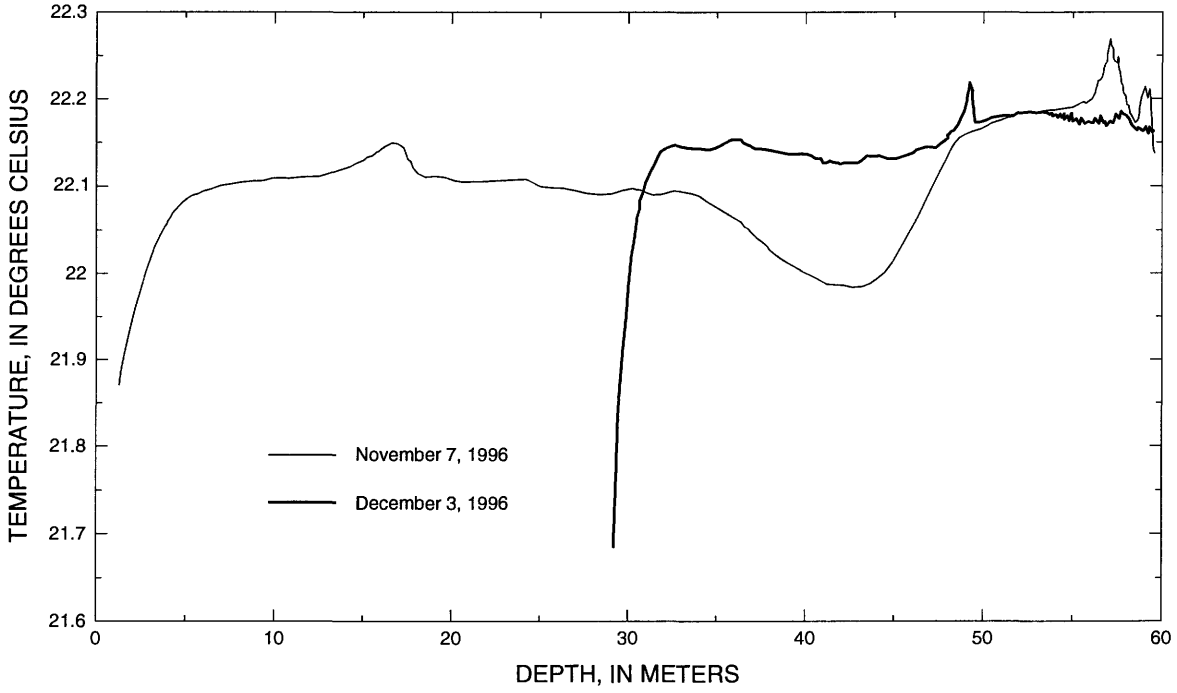

Figure 7. Temperature plot showing the geothermal logs from borehole NAD-GTB#1a.

Results from Pneumatic Pressure Monitoring in Borehole NAD-GTB#1a

A schematic diagram of borehole NAD-GTB#1a and the locations of the isolated downhole-monitor intervals used for pneumatic monitoring are shown in figure 8. The liner was installed to maximize the number of monitor intervals that intersected the 12-m-wide broken zone (143 to 155 m measured from the ESF centerline) that had been identified in the borehole video log. The barometric pressure and the downhole-monitor interval pressures for December 26 to 31, 1996 (DTN: GS970283122410.003), are shown in figure 9. The downhole-monitor interval pressures identified limited barometric pressure attenuation and small time lags. Comparison of the downhole-monitor intervals pressure fluctuations (0.56 to 0.83 kPa) to the barometric-pressure fluctuation (1.07 kPa) indicated that the permeability of the rock is relatively high. Monitor intervals 2, 3, and 7 had the smallest attenuations. Monitor intervals 4, 6, 8, and 9 had the largest attenuations, and monitor intervals 1, 5, and 10 had intermediate attenuations. Pressure monitoring showed no correlation between the amount of pressure attenuation and the distance from the NAD and no correlation between pressure attenuation and the distance from the main trace of the GDF. The amount of attenuation shows no pattern and may be random. The randomness may be due to the small size of the downhole-monitor intervals (borehole-surface-contact area of approximately 0.07 m^2). The small monitor interval area may result in the downhole-monitor intervals contacting the borehole at locations that do not have fractures and, therefore, are not well connected to the fracture system. A poor connection to the fracture system may explain why monitor interval 1, which was closest to the NAD, had a larger attenuation than monitor intervals 2 and 3, which are at greater distances from the NAD and would be expected to have larger pressure attenuations. Monitor interval 10 was the farthest from the NAD and, therefore, would be expected to have the largest attenuation of the NAD barometric-pressure change. The intermediate attenuation measured in monitor interval 10 may indicate that the barometric pressure changes were transmitted from the ground surface through the GDF to depth. The larger attenuation measured in monitor interval 9, which also was close to the main trace of the fault, may be due to the small monitor interval area and to a poor connection to the fracture system. The noise recorded in monitor interval 5 was probably due to a faulty solenoid valve.

Results from Chemical Sampling in Borehole NAD-GTB#1a

The results of the chemical analysis of the gas-phase samples from borehole NAD-GTB#1a are presented in table 2. (DTN: GS970283122410.002) During the drilling of borehole NAD-GTB#1a, an error in the operation of the SF_6 tracer-gas-injection

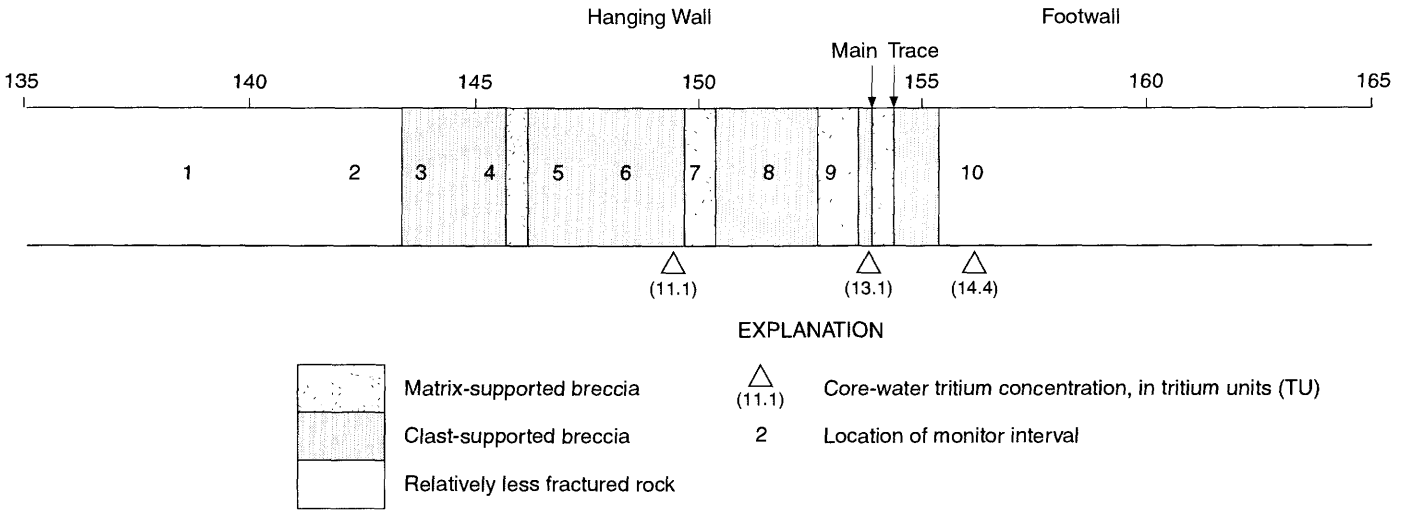

Figure 8. Schematic diagram showing borehole NAD-GTB#1a intersection with the Ghost Dance Fault and the locations of the downhole-monitor intervals.

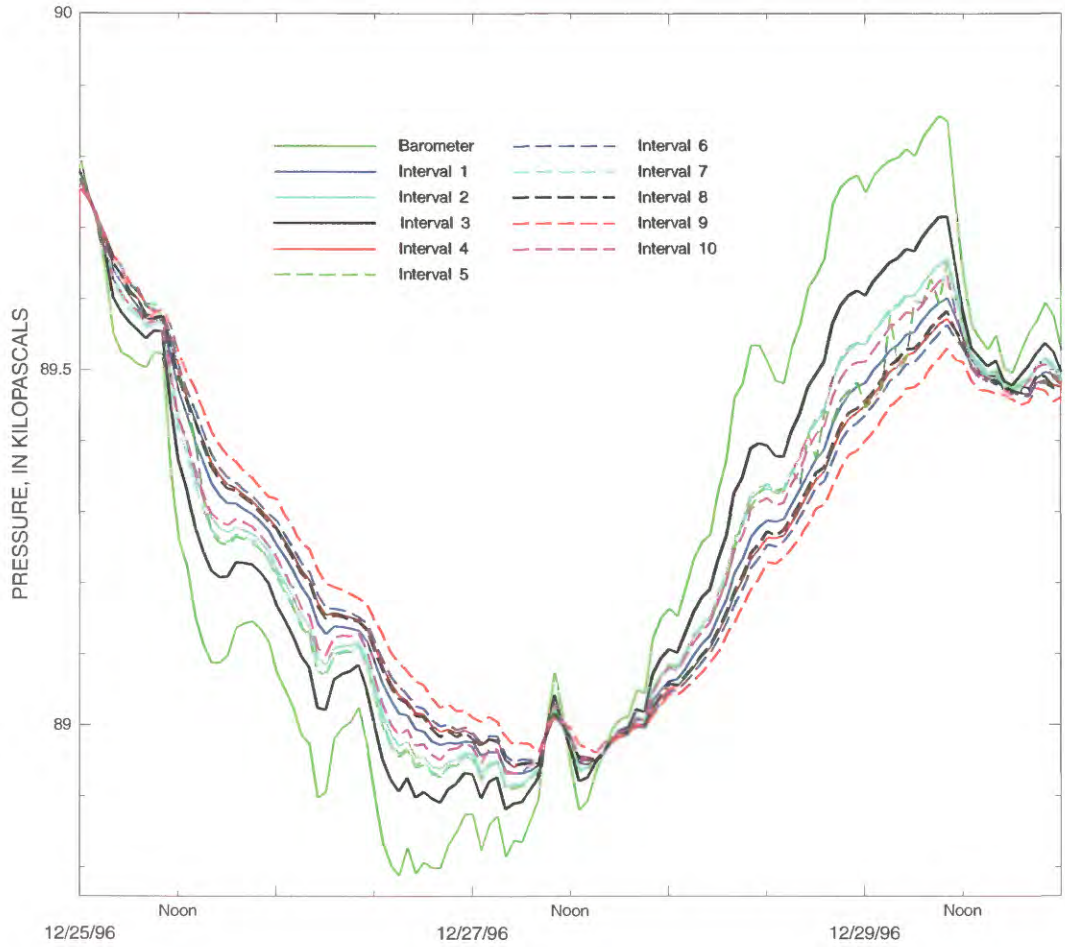

Figure 9. Barometric pressure and the pressure responses in the isolated intervals in borehole NAD-GTB#1a.

system occurred. On November 1, 1996, at the drilling depth of 160.5 to 161.5 m, the valve on the SF_6 tracer-gas cylinder was opened, and about 800 liters (L) of 10-percent SF_6 was pumped into the borehole. The presampling pumping period was extended in an attempt to remove the excess SF_6. Final SF_6 concentrations in 7 of the 10 monitor intervals were less than 0.01 ppm (table 2), indicating that the presample pumping removed most of the drilling air. The higher SF_6 concentrations in monitor intervals 6, 9, and 10 (0.058, 0.815, and 0.030 ppm) may be associated with the large pneumatic attenuations measured in monitor intervals 6, and 9. The elevated SF_6 values may be due to restricted presampling pumping rates due to poor connections to the fracture system and low tuff matrix permeability, or may be due to sorption of SF_6 by the tuff matrix or fault breccia. Monitor interval 10 had a residual SF_6 concentration of 0.030, but unlike monitor intervals 6 and 9, monitor interval 10 had an intermediate pressure attenuation and does not fit the model. Although monitor interval 9 had the largest SF_6 concentration, it also had the lightest $\delta^{13}C$ ratio (-16.18) and the oldest ^{14}C age (4,500 years) (table 2). The carbon values indicated that the presampling pumping had removed most of the drilling air from monitor interval 9.

Gas-phase CO_2 concentrations ranged from 660 to 1,175 ppm (table 2). The CO_2 values increased with

Table 2. Results of the chemical analysis of the gas-phase samples from borehole NAD-GTB#1a

[ppm, parts per million; PDB, Pee Dee Belemnite; ‰, parts per thousand; pmc, percent modern carbon; %, percent]

Monitor interval	Depth (meters)	SF_6 (ppm)	CO_2 (ppm)	$\delta^{13}C$ (‰) (standard is PDB)	^{14}C (pmc)	^{14}C age (years)	^{14}C age ±(%)
1	139.1	0.001	713.0	-14.18	69	3,100	1.0
2	142.2	0.000	660.0	-14.11	75	2,400	1.2
3	143.7	0.000	711.0	-14.17	72	2,700	1.8
4	145.2	0.001	925.0	-15.10	64	3,700	0.8
5	146.8	0.004	996.0	-15.46	67	3,300	1.0
6	148.3	0.058	976.0	-15.39	68	3,200	1.4
7	149.8	0.000	1,075.0	-15.58	71	2,800	1.3
8	151.3	0.008	1,079.0	-14.81	61	4,100	0.8
9	152.9	0.815	1,175.0	-16.18	58	4,500	1.0
10	155.9	0.030	1,067.0	-15.89	66	3,400	0.7

distance from the NAD ($r = 0.89$). The correlation indicated that NAD air had moved a minimum of 13.9 m into the tuff. Monitor intervals 1, 2, and 3 had the lowest CO_2 concentrations and slightly heavier $\delta^{13}C$ ratios, indicating the highest component of NAD gas. Both the low CO_2 and the slightly heavier $\delta^{13}C$ ratios are probably due to the close location of monitor intervals 1, 2, and 3 to the NAD and to the subsequent mixing of the rock gas with NAD air. As discussed in the pneumatic monitoring section, monitor intervals 2 and 3 had minimal pressure attenuation, supporting the concept of a well-developed fracture connection to the NAD. Gas-phase $\delta^{13}C$ values decreased with distance from the NAD ($r = 0.84$), again indicating that air from the NAD has penetrated the tuff.

Uncorrected ^{14}C-age estimates from gas samples ranged from 2,400 to 4,500 years (table 2). Monitor intervals 2, 3, and 7, which had the minimum pressure attenuations, had ^{14}C-age estimates of 2,400, 2,800, and 2,900 years, respectively. Monitor intervals 1, 5, and 10, which had intermediate pressure attenuations, had ^{14}C-age estimates of 3,000, 3,300, and 3,400 years, respectively. Monitor intervals 4, 6, 8, and 9, which had the maximum pressure attenuations, had ^{14}C-age estimates of 3,700, 3,200, 4,000, and 4,500 years, respectively. The ^{14}C-age estimates of the monitor intervals are directly correlated to the amount of pressure attenuation measured during pneumatic monitoring ($r = 0.75$, ranked 1 to 10 with 1 the smallest pressure attenuation). The age/attenuation correlation indicated that air from the NAD had penetrated the tuff through the fracture system.

The results of the tritium analysis of water distilled from core samples from borehole NAD-GTB#1a (DTN: GS970283122410.002, and DTN: GS990183122410.001) are listed in table 3. The table 3 tritium analysis results are classified non-quality assured. Eight samples at six depths had tritium levels that were significant at two standard deviations. The eight samples each has a 95.4-percent probability of being greater than zero and, therefore, positive for tritium. Assuming that the tritium levels are not due to contamination, the presence of measurable tritium indicates that water has been transported from the ground surface to the depth of the NGDFA during about the last 100 years (8 half-lives).

There are few reliable estimates of the natural tritium levels in the atmosphere before the 1952 advent of atmospheric thermonuclear testing greatly increased the tritium background levels. Best estimates of tritium levels in pre-1952 precipitation vary with location and season but are in the range of 4 to 25 tritium units (TU) (Fritz and Fontes, 1980, p. 22). By using a conservative assumption that pre-1952 precipitation at Yucca Mountain had a tritium content of 25 TU, and by using a tritium half-life of 12.3 years, the 1997 tritium content of core water from borehole NAD-GTB#1a that was derived from 1952 precipitation would be 2.0 TU. Therefore, some component of the water in core-water samples, which

Table 3. Results of the tritium analysis of core-water samples from borehole NAD-GTB#1a (These data are classified as non-quality assured)

Distance from exploratory studies facility centerline (meters)	Tritium units (TU)	Standard deviation	Tritium units minus two standard deviations
135.3[1]	1.4	0.4	0.6
142.1	-2.5	2.9	0
142.4[1]	1.2	0.4	0.4
143.1[1]	1.2	0.4	0.4
143.5	5.2	3.0	0
144.5	-1.4	2.9	0
144.9[1]	0.8	0.7	0
145.4	0.3	3.0	0
146.2	-0.2	4.4	0
147.5[1]	0.3	0.4	0
148.3	1.1	3.0	0
148.9	11.1	4.1	2.9
148.9[2]	8.6	4.1	0.4
149.9	0.6	3.0	0
150.4	5.4	3.0	0
151.1	6.3	4.0	0
151.7	4.3	4.0	0
152.0	6.3	4.1	0
152.0	2.4	4.1	0
154.4	9.2	4.1	1.0
154.9	5.1	4.0	0
155.0	7.3	4.0	0
155.0	2.2	4.0	0
155.2	12.2	4.2	3.8
155.2[2]	14.4	4.2	6.0
156.4[1]	0.8	0.5	0

[1]Analysis by the University of Miami, Miami, Florida.
[2]Replicate sample.

had tritium levels greater than 2.0 TU, had some contact with the atmosphere in the last 45 years (post-1952 atmospheric thermonuclear testing). Three core-water samples at two depths had tritium values greater than 2.0 TU at two standard deviations (table 3). These tritium values indicated that water had traveled from the land surface to the depth of the borehole in the last 45 years. The proximity of the elevated tritium samples to the main trace of the GDF and to the 12-m-wide broken zone (fig. 8) indicated that the fault is a conduit for the transport of water from the land surface through the nonwelded tuff of the Paintbrush Group and down to the Tptpmn. A less conservative approach assumes that the pre-1952 precipitation at Yucca Mountain had a tritium content of 4 TU. By using a pre-1952 tritium level of 4 TU, the 1997 tritium content of core water from borehole NAD-GTB#1a that was derived from 1952 precipitation would be 0.32 TU. This less conservative approach indicated that the eight core-water samples that were positive for tritium at two standard deviations (table 3) have a component of post-1952 water. However, interpretation of tritium levels as low as 0.4 to 1.0 TU requires consideration of the possibility that the samples were contaminated during drilling, core logging, or packaging and shipping. As tritium levels decrease and significance is assigned, the effect of even short periods of atmospheric exposure and small

amounts of contamination becomes larger. The actual tritium levels from pre-1952 precipitation at Yucca Mountain probably are between 4 and 25 TU and vary with the seasons. In summary, the core-water tritium data from borehole NAD-GTB#1a indicated that the fault is a conduit for the rapid transport (less than 100 years) of water from the land surface to the Tptpmn.

Results from Chemical Sampling in the Northern Drill Room Boreholes

The results of the chemical analysis of the gas-phase samples from borehole MF#1 are listed in table 4. Gas-phase CO_2 concentrations in borehole NAD-MF#1 (DTN: GS981283122410.006) ranged from 741 to 913 ppm. Gas-phase $\delta^{13}C$ values ranged from -14.79 to -13.81 per mil. Gas-phase ^{14}C ages ranged from 2,500 to 3,600 years. There was no correlation between the parameters and depth. The monitor interval centered at 12.5 m was in the footwall, and the monitor intervals centered at 18.6, 21.6, and 24.7 m were in the hanging wall. The monitor interval centered at 15.5 m was located in the fault zone. The data indicate that the gas samples are a mixture of NGDFA air and rock gas. The monitor interval centered at 15.5 m had the lowest CO_2, largest $\delta^{13}C$, and youngest ^{14}C age, all indicating that the gas sample from the fault zone had the greatest mixing with NGDFA air. The mixing was probably due to (1) the high permeability of the fault zone, as identified in the air-injection testing; (2) the NAD penetration of the fault, providing a short flow path; and (3) the 17 months that elapsed between the NAD penetration of the fault in March 1997 and gas sampling in August 1998.

The results of the chemical analysis of the gas-phase samples from borehole NDR-MF#2 are listed in table 5. Gas-phase CO_2 concentrations in borehole NDR-MF#2 (DTN: GS981283122410.006) ranged from 711 to 896 ppm. Gas-phase $\delta^{13}C$ values ranged from -15.04 to -13.45 per mil. Gas-phase ^{14}C ages ranged from 2,600 to 3,500 years. There is no correlation between the parameters and depth. The monitor interval centered at 12.2 m was in the footwall, and the monitor intervals centered at 18.3, 21.3, and 24.4 m were in the hanging wall. The monitor interval centered at 15.2 m was in the fault zone. The data indicated that the gas samples are a mixture of NGDFA air and rock gas. The monitor interval centered at 15.2 m had the lowest CO_2, second largest $\delta^{13}C$, and largest percent modern carbon, all indicating that the gas sample from the fault zone had the greatest mixing with NGDFA air. The mixing was probably due to (1) the high permeability of the fault zone, as identified in the air-injection testing; (2) the NAD penetration of the fault, providing a short flow path; and (3) the 17 months that elapsed between NAD penetration of the fault in March 1997 and gas sampling in August 1998.

The results of the tritium analysis done by the University of Miami of core-water samples from borehole NDR-MF#1 (DTN: GS990183122410.004) are listed in table 6. The table 6 tritium analysis results are classified as non-quality assured. The monitor interval centered at 13.8 m was in the footwall, and the monitor interval centered at 15.2 m was in the fault zone. Both samples had tritium levels that were signif-

Table 4. Results of the chemical analysis of gas-phase samples from borehole NDR-MF#1

[ppm, parts per million; PDB, PeeDee Belemnite; ‰, parts per thousand; pmc, percent modern carbon; %, percent]

Depth (meters)	CO_2 (ppm)	$\delta^{13}C$ (‰) (standard is PDB)	^{14}C (pmc)	^{14}C age (years)	^{14}C age ±(%)
12.5	870	-14.3	72	2,700	1.3
15.5	741	-13.8	74	2,500	2.5
18.6	884	-14.6	71	2,800	2.1
21.6	913	-14.8	65	3,600	1.4
24.7	743	-14.4	71	2,800	2.0

Table 5. Results of the chemical analysis of gas-phase samples from borehole NDR-MF#2

[ppm, parts per million; PDB, Pee Dee Belemnite; ‰, parts per thousand; pmc, percent modern carbon; %, percent]

Depth (meters)	CO_2 (ppm)	$\delta^{13}C$ (‰) (standard is PDB)	^{14}C (pmc)	^{14}C age (years)	^{14}C age ±(%)
12.2	736	-13.4	73	2,600	0.8
15.2	711	-13.5	73	2,600	1.6
18.3	777	-14.1	65	3,600	1.4
21.3	836	-15.0	73	2,600	1.9
24.4	896	-15.0	66	3,400	0.7

icant at two standard deviations and have 95.4 percent probabilities of being greater than zero and positive for tritium. Assuming that the tritium levels are not due to contamination, the presence of measurable tritium indicates that water has been transported from the ground surface to the borehole in about the last 100 years (8 half-lives). Using the conservative assumption that pre-1952 precipitation at Yucca Mountain had a tritium content of 25 TU, the data do not indicate post-1952 water. Using a pre-1952 tritium level of 4 TU, the data indicated that both borehole NDR-MF#1 core-water samples have a component of post-1952 water. In summary, the core-water sample tritium values from borehole MF#1 indicated that the fault is a conduit for the rapid transport (< 100 years) of water from the land surface through the nonwelded tuff of the Paintbrush Group and down to the Tptpmn.

Results from Single-Hole Air-Injection Testing in Borehole NAD-GTB#1a

The permeability values from single-hole air-injection testing in borehole NAD-GTB#1a (DTN: GS970383122410.004) are presented in table 7. Air-injection testing identified three zones that had different permeability values. The three zones correspond to the structural units: footwall, hanging wall, and a high-permeability fault zone similar to that identified in the NDR boreholes. The fault zone in GTB#1a is a subsection of the 12-m-wide broken zone. The fault zone extends from 15.0 to 18.4 m and is composed of a brecciated zone associated with the main trace of the fault and the adjacent, intensely fractured hanging wall. Permeability values from the hanging wall ranged from 0.1 to 2.5×10^{-12} m^2 and had an arithmetic mean of 1.1×10^{-12} m^2 and a geometric mean of 0.5×10^{-12} m^2. The fault zone permeability values ranged from 8.5 to 11.1×10^{-12} m^2 and had arithmetic and geometric means of 10.0×10^{-12} m^2. The permeability values of the footwall ranged from 0.2 to, 2.1×10^{-12} m^2 and had an arithmetic mean of 1.0×10^{-12} m^2 and a geometric mean of 0.7×10^{-12} m^2. The permeability value of the 12-m-long test interval that straddled the hanging wall, fault zone, and footwall was 5.7×10^{-12} m^2. The mean permeability values of the Tptpmn from the surface-based air-injection testing ranged from 0.37 to 2.7×10^{-12} m^2 (LeCain, 1997, p. 23). Comparison of the permeability values from borehole NAD-GTB#1a to the surface-based values indicated that the permeability values for the hanging wall and the footwall are in the surface-based range, but the fault-zone permeability values are several factors larger. The most probable explanation for the increased permeability in the fault zone is increased fracturing associated with the GDF.

Table 6. Results of the University of Miami tritium analysis of core-water samples from borehole NDR-MF#1 (These data are classified as non-quality assured)

Depth (meters)	Tritium units (TU)	Standard deviation	Tritium units minus two standard deviations
13.8	1.6	0.5	0.6
15.2	2.2	0.6	1.0

Table 7. Permeability values from air-injection testing in borehole NAD-GTB#1a (These tests were done when the northern access drift face was located at 134.4 meters from the ESF)

[Permeability values are 10^{-12} meter squared]

Depth (meters)	Structural unit	Permeability values
1.9-2.9	Hanging wall	0.1
2.8-3.8	Hanging wall	0.6
6.5-7.5	Hanging wall	0.1
8.3-9.3	Hanging wall	2.5
13.2-14.2	Hanging wall	2.3
15.0-16.0	Hanging wall (fault zone)	11.1
15.8-16.8	Hanging wall (fault zone)	8.5
17.4-18.4	Brecciated zone (fault zone)	10.5
18.7-19.7	Footwall	2.1
19.6-20.6	Footwall	1.3
21.1-22.1	Footwall	0.5
22.3-23.2	Footwall	0.2
8.7-20.7	Hanging wall-Brecciated zone-Footwall	5.7

Results from Cross-Hole Air-Injection Testing in the Northern Drill Room Boreholes

Analysis Using Type Curves

The initial examination of the pressure responses in the monitor intervals identified three zones that had different pressure responses. These three zones correspond to the structural units: footwall, fault zone, and hanging wall. The normalized pressure responses and theoretical type curves for monitor intervals located in the footwall, fault zone, and hanging wall are shown in figures 10, 11, and 12, respectively. In a homogeneous and isotropic medium, the normalized pressure plots would form a single curve. In a heterogeneous medium, the pressure data from monitor intervals in highly permeable zones will have an early t/r^2 response and the less permeable zones will have a delayed t/r^2 response. Directional effects would be identified as pressure variability increasing in the direction of lower permeability. Although the curves in figures 10, 11, and 12 are not perfectly matched, they are very similar, and with a few exceptions the pressure responses are within a factor of two; the pressure variability may indicate that the test scale was smaller than the representative elementary volume. The normalized pressure responses indicated no correlation between pressure response and direction. The identification of three zones with different pneumatic characteristics, and the absence of directional effects, indicated that the northern GDF test area was heterogeneous with three zones of different permeability and that the three zones were isotropic.

Following the initial examinations, the pressure responses of the monitor intervals were analyzed using spherical- and radial-flow type curves. The analysis assumed that the matrix was water filled; this is reasonable because no delayed storage components were identified in the pressure responses. Tests done in the footwall and hanging wall best matched the spherical-flow model. Tests done in the fault zone best matched a radial-flow model; the data also indicated some leakage. The radial-flow model best matched the fault zone because the higher permeability fault zone was bounded by the lower permeability footwall and hanging wall, which restricted the gas flow to a leaky-radial-flow geometry. The permeability and porosity values from the type-curve analysis are presented in tables 8 through 12. Statistical summaries of the permeability and porosity values by structural unit are presented in tables 13 and 14. The pressure responses and locations of the monitor intervals for the individual cross-hole air-injection tests are available in the YMP data packages DTN: GS980183122410.001 and GS981183122410.005.

Statistical summaries of the permeability and porosity values from the type-curve analytical solutions of cross-hole air-injection testing are listed in tables 13 and 14. The arithmetic mean permeability and porosity values of the three structural units are: footwall 8.7×10^{-12} m^2, and 0.04; fault zone 18.1×10^{-12} m^2, and 0.13; hanging wall 5.0×10^{-12} m^2, and 0.04. The type-curve analysis indicated that the permeability and porosity values of the three individual structural units were independent of direction. The analysis identified boundary effects when the monitor interval and the air-injection interval were located in different structural units, and when a monitor interval was located immediately adjacent to an adjoining structural unit. The type-curve analysis identified a heterogeneous flow system that had three

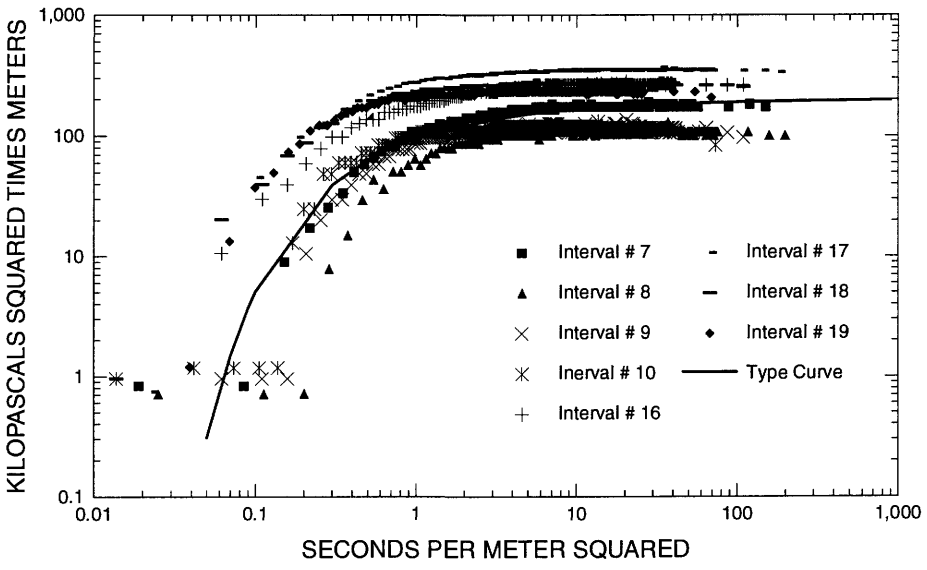

Figure 10. Pressure response times distance, with time, divided by distance squared measured in the footwall during cross-hole air-injection test 22, and the type curve for spherical flow.

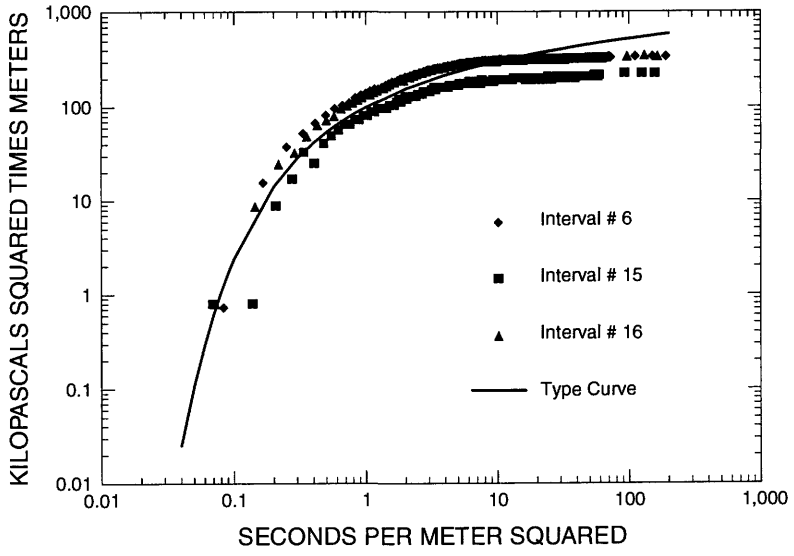

Figure 11. Pressure response times distance, with time, divided by distance squared measured in the fault zone during cross-hole air-injection test 16, and the type curve for radial flow.

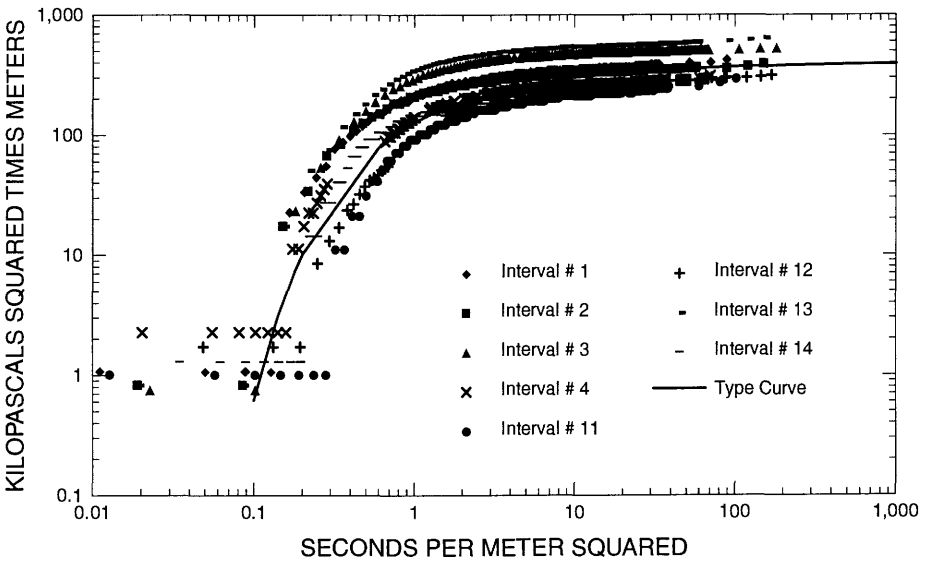

Figure 12. Pressure response times distance, with time, divided by distance squared measured in the hanging wall during cross-hole air-injection test 19, and the type curve for spherical flow.

different homogeneous isotropic structural units corresponding to the footwall, fault zone, and hanging wall. Comparison of the NDR cross-hole permeability values to the single-hole permeability values from borehole NAD-GTB#1a indicates reasonable agreement between the arithmetic means for the fault zone (values within a factor of 2) but differences approaching a factor of 5 in the hanging wall and almost an order of magnitude in the footwall. The permeability differences may be real or they may be a scale effect due to the smaller test scale of the single-hole GTB#1a testing. Overall, the NGDFA cross-hole permeability values for the Tptpmn are larger than the range of the surface-based permeability values for the Tptpmn (0.37 to 2.7×10^{-12} m^2) (LeCain, 1997, p. 23). The increased permeability is probably due to increased fracturing associated with the GDF. Although the monitor interval pressure responses did not indicate a dual-porosity system, and the analysis assumed that the matrix was water filled, the porosity values were greater than expected and indicate a porosity component in addition to the fracture porosity. Fracture porosity generally ranges from 10^{-2} to 10^{-5} (Freeze and Cherry, 1979, p. 408). Visual examinations in the NAD indicated that the fault-zone fracture porosity may be larger than 10^{-2}. Possible explanations of the additional porosity include air-filled lithophysal cavities and/or air-filled matrix pores in direct contact with the fractures.

Numerical Analysis Using AIR3D

By using geologic information from the DLS, geologic mapping, visual inspection of the NAD and NDR, and borehole video logs, a numerical model of the northern GDF flow system was developed using the USGS finite-difference model AIR3D (Joss and Baehr, 1995). The numerical model grid was 40 layers, 25 columns, and 25 rows. The model layer thickness was a constant 2 m, while the column and row widths ranged from 0.1 m, at the central nodes, up to 10.0 m at the outer boundaries. The X, Y, Z scale of the model was 76.1 by 76.1 by 80.0 m, respectively. The lower boundary was no flow (representing the water table) and the other five boundaries were constant head. To minimize boundary effects, the model scale was large compared to the field-testing scale. The footwall was assigned layers 1 through 20, the fault zone layers 21 and 22, and the hanging wall layers 23 through 40. The relative locations of the model air-injection and monitor intervals were selected to match the field tests. The initial model run used the arithmetic-mean permeability and porosity values from the type-curve analysis for the footwall, fault zone, and hanging wall. Pressure responses from the numerical model were visually compared to the pressure responses from field testing. By using these comparisons, the permeability and porosity values of the model were adjusted and the model was rerun; the model pressure responses again were compared to the

Table 8. Permeability and porosity values from cross-hole air-injection testing using borehole NDR-MF#2 for injection and borehole NDR-MF#1 for monitoring

[Permeability values are 10^{-12} meter squared; porosity is in parentheses; --, no data; FZ, fault zone; PFZ, partial fault zone, defined as a monitor interval located in the fault zone and footwall]

Test number	Injection interval depth (meters)	Injection interval structural unit	Permeability and porosity values from monitor intervals located in borehole NDR-MF#1									
			Hanging Wall					FZ	PFZ		Footwall	
			1	2	3	4	5	6	7	8	9	10
1	25.9-30.6	Hanging wall	5.1	5.9	6.3	--	--	--	--	--	--	--
			(.03)	(.07)	(.06)	--	--	--	--	--	--	--
2	25.9-28.9	Hanging wall	5.4	7.0	6.5	--	--	--	--	--	--	--
			(.03)	(.05)	(.05)	--	--	--	--	--	--	--
3	22.8-25.9	Hanging wall	3.8	3.7	3.3	4.7	--	--	--	--	--	--
			(.01)	(.01)	(.02)	(.06)	--	--	--	--	--	--
4	21.3-24.3	Hanging wall	2.0	1.5	1.3	1.2	--	--	--	--	--	--
			(.01)	(.01)	(.01)	(.06)	--	--	--	--	--	--
5	19.2-22.2	Hanging wall	1.4	0.8	0.7	0.7	1.3	--	--	--	--	--
			(.01)	(.01)	(.02)	(.04)	(.07)	--	--	--	--	--
6	15.2-18.3	Fault zone	--	--	--	0.9	0.7	9.2	18.1	--	--	--
			--	--	--	(.03)	(.02)	(.15)	(.17)	--	--	--
7	11.6-14.6	Partial fault zone	--	--	--	--	13.2	5.1	9.4	17.2	--	--
			--	--	--	--	(.14)	(.05)	(.11)	(.18)	--	--
8	8.8-11.9	Footwall	--	--	--	--	--	9.3	9.4	12.0	10.7	10.8
			--	--	--	--	--	(.05)	(.06)	(.04)	(.03)	(.02)
9	5.2-8.2	Footwall	--	--	--	--	--	14.4	1.1	6.2	5.1	6.4
			--	--	--	--	--	(.06)	(.02)	(.05)	(.05)	(.05)
10	3.7-6.7	Footwall	--	--	--	--	--	10.5	6.7	5.4	4.3	5.5
			--	--	--	--	--	(.04)	(.03)	(.04)	(.05)	(.06)
11	1.5-4.5	Footwall	--	--	--	--	--	--	--	9.8	6.2	8.9
			--	--	--	--	--	--	--	(.05)	(.03)	(.05)

Table 9. Permeability and porosity values from cross-hole air-injection testing using borehole NDR-MF#3 for injection and borehole NDR-MF#1 for monitoring

[Permeability values are 10^{-12} meter squared; porosity is in parentheses; --, no data; FZ, fault zone; PFZ, partial fault zone, defined as a monitor interval located in the fault zone and footwall]

Test number	Injection interval depth (meters)	Injection interval structural unit	Permeability and porosity values from monitor intervals located in borehole NDR-MF#1									
			Hanging Wall					FZ	PFZ		Footwall	
			1	2	3	4	5	6	7	8	9	10
12	26.4-34.3	Hanging wall	6.2	8.0	5.4	8.0	--	--	--	--	--	--
			(.04)	(.06)	(.04)	(.06	--	--	--	--	--	--
16	12.3-17.3	Fault zone	--	--	--	25.3	15.3	7.0	13.2	22.2	19.7	--
			--	--	--	(.30)	(.15)	(.05)	(.16)	(.22)	(.16)	--
17	3.5-8.5	Footwall	--	--	--	--	--	13.2	9.3	9.9	7.0	8.1
			--	--	--	--	--	(.05)	(.03)	(.04)	(.03)	(.03)
19	24.5-26.5	Hanging wall	5.7	6.1	3.6	5.7	12.4	--	--	--	--	--
			(.03)	(.03)	(.03)	(.06)	(.02)	--	--	--	--	--
21	18.5-20.5	Hanging wall	5.4	6.0	3.8	--	3.5	21.9	--	--	--	--
			(.02)	(.03)	(.02)	--	(.08)	(.40)	--	--	--	--
22	8.7-10.7	Footwall	--	--	--	--	--	9.3	10.1	15.9	11.8	13.6
			--	--	--	--	--	(.05)	(.07)	(.12)	(.07)	(.05)
23	3.2-5.2	Footwall	--	--	--	--	--	13. 4	10. 8	10. 8	4.4	5.2
			--	--	--	--	--	(.0 4	(.0 3)	(.0 3)	(.0 1)	(.0 1)

Table 10. Permeability and porosity values from cross-hole air-injection testing using borehole NDR-MF#3 for injection and borehole NDR-MF#2 for monitoring

[Permeability values are 10^{-12} meter squared; porosity is in parentheses; --, no data; FZ, fault zone; PFZ, partial fault zone, defined as a monitor interval located in the fault zone and footwall]

Test number	Injection interval depth (meters)	Injection interval structural unit	Permeability and porosity values from monitor intervals located in borehole NDR-MF#2									
			Hanging Wall					FZ	PFZ		Footwall	
			11	12	13	14	15	16	17	18	19	20
12	26.4-34.3	Hanging wall	7.5	5.3	4.9	12.8	--	--	--	--	--	--
			(.06)	(.06)	(.03)	(.07	--	--	--	--	--	--
16	12.3-17.3	Fault zone	--	--	--	20.0	10.4	6.6	11.5	13.3	--	--
			--	--	--	(.23)	(.09)	(.05)	(.05)	(.06)	--	--
17	3.5-8.5	Footwall	--	--	--	--	--	12.0	5.4	5.5	5.3	--
			--	--	--	--	--	(.04)	(.01)	(.02)	(.02)	--
19	24.5-26.5	Hanging wall	8.0	5.9	2.7	7.4	13.2	--	--	--	--	--
			(.09)	(.09)	(.02)	(.05)	(.05)	--	--	--	--	--
21	18.5-20.5	Hanging wall	8.0	6.0	4.2	--	3.3	20.0	--	--	--	--
			(.04)	(.05)	(.04)	--	(.03)	(.22)	--	--	--	--
22	8.7-10.7	Footwall	--	--	--	--	12.7	8.4	5.2	6.3	6.9	--
			--	--	--	--	(.10)	(.02)	(.02)	(.02)	(.02)	--
23	3.2-5.2	Footwall	--	--	--	--	--	13.3	8.2	7.9	7.7	34.1
			--	--	--	--	--	(.04)	(.02)	(.03)	(.03)	(.10)

Table 11. Permeability and porosity values from cross-hole air-injection testing using borehole NDR-MF#1 for injection and borehole NDR-MF#3 for monitoring

[Permeability values are 10^{-12} meter squared; porosity is in parentheses; --, no data; FZ, fault zone; PFZ, partial fault zone, defined as a monitor interval located in the fault zone and footwall]

Test number	Injection interval depth (meters)	Injection interval structural unit	Permeability and porosity values from monitor intervals bore located in borehole NDR-MF#3									
			Hanging Wall					FZ	PFZ		Footwall	
			1	2	3	4	5	6	7	8	9	10
25	25.8-27.8	Hanging wall	5.1	4.0	4.9	3.1	8.8	--	--	--	--	--
			(.02)	(.03)	(.04)	(.02)	(.07)	--	--	--	--	--
32	13.3-15.3	Fault zone	--	--	--	31.4	12.2	26.1	27.3	9.0	15.3	--
			--	--	--	(.10)	(.14)	(.07)	(.07)	(.06)	(.07)	--
36	5.5-7.5	Footwall	--	--	--	--	--	15.5	16.2	9.9	10.0	--
			--	--	--	--	--	(.05)	(.20)	(.05)	(.06)	--

Table 12. Permeability and porosity values from cross-hole air-injection testing using borehole NDR-MF#1 for injection and borehole NDR-MF#2 for monitoring

[Permeability values are 10^{-12} meter squared; porosity is in parentheses; --, no data; FZ, fault zone; PFZ, partial fault zone, defined as a monitor interval located in the fault zone and footwall]

Test number	Injection interval depth (meters)	Injection interval structural unit	Permeability and porosity values from monitor intervals located in borehole NDR-MF#2									
			Hanging Wall					FZ	PFZ		Footwall	
			11	12	13	14	15	16	17	18	19	20
25	25.8-27.8	Hanging wall	5.8	4.0	2.2	6.1	17.2	--	--	--	--	--
			(.04)	(.04)	(.01)	(.03)	(.10)	--	--	--	--	--
32	13.3-15.3	Fault zone	--	--	--	20.8	37.9	27.3	11.5	15.7	16.5	--
			--	--	--	(.19)	(.27)	(.08)	(.06)	(.06)	(.06)	--
36	5.5-7.5	Footwall	--	--	--	--	23.6	11.7	9.6	8.8	9.3	--
			--	--	--	--	(.16)	(.06)	(.04)	(.04)	(.04)	--

Table 13. Statistical summary of permeability values from the type-curve analytical solutions of cross-hole air-injection testing of the northern Ghost Dance Fault

[Permeability values are 10^{-12} meter squared]

Structural unit	Permeability values arithmetic mean	Permeability values range	Permeability values geometric mean
Hanging wall	5.0	0.7-12.8	4.1
Fault zone	18.1	7.0-37.9	14.6
Footwall	8.7	1.1-34.1	7.8

pressure responses from the field. This iterative process was repeated until a qualitative best match between the pressure responses from the model and the pressure responses from the field testing was obtained. The pressure responses from three monitor intervals of field test 16 and the AIR3D numerical model predicted pressure response are presented in figure 13. The three monitor intervals were located in the fault zone at distances of 4.4, 4.5 and 4.1 meters from the air-injection interval. The numerical model predicted pressure response is for a linear distance of 4.5 m. The numerical model used a fault-zone permeability value of 20×10^{-12} m^2 and porosity value of 0.20, which were ultimately selected as the values providing the qualitative best match.

The AIR3D numerical model permeability and porosity values that best matched the observed field-test pressure responses are: footwall 10.0×10^{-12} m^2, and 0.07; fault zone 20.0×10^{-12} m^2, and 0.20; hanging wall 5.0×10^{-12} m^2, and 0.05. These values are very similar to the type-curve values and indicate close agreement between the two methods; however, there are additional considerations. The pressure responses from the numerical model replicated the field data from the fault zone more accurately than the data from the footwall and the hanging wall. The early-time field data (< 100 seconds) from the footwall are a closer match when the model-footwall permeability and porosity values are 5.0×10^{-12} m^2 and 0.05. The same is true for the hanging wall where permeability and porosity values of 3.0×10^{-12} m^2, and 0.03 provide a better fit to the early-time field data. However, the late-time field data (>100 seconds) indicated a higher permeability and porosity; therefore, the best-match permeability and porosity values are a compromise to best fit both the early- and late-time data. An alternative model would use the lower permeability values for the hanging wall and the footwall and would assume a constant-head boundary, such as a large fracture, to account for the late-time rapid stabilization of the pressure responses. Because the field work (geologic mapping, fracture mapping, borehole logging, and air-injection testing) does not indicate any physical feature that could act as a constant-head boundary, a compromise needs to be made; therefore, the best-match permeability and porosity values are a reasonable match to the field data. Other possible interpretations include a high-permeability connection of the fracture system to the NDR and the NDR is the constant head boundary—or possibly the footwall and hanging wall would be better represented using a dual-porosity model. As already noted, the pressure responses did not indicate a dual-porosity system (no delayed storage); however, the large porosity values indicate that the assumption of a water-saturated matrix may be questionable.

Discrete-Feature Analysis Using FRACMAN

The CLUSTRAN analysis identified six statistically significant fracture groups in the NGDFA. The strike and dip of the fracture planes in degrees are: 059/88, 075/84, 125/84, and 332/63; minor subsets are at 192/87 and 199/63. The fractures are moderately to steeply inclined, trend in a northerly and in a northwesterly direction, and have nonuniform spacing. There was no apparent correlation between length and orientation, even though fractures that parallel the NGDFA had a greater probability of having long lengths. The analysis indicated that the fracture lengths follow log-normal, power law, and exponential distributions. The six fracture sets, and their statistical parameters were used as input to the FRACSYS algorithm of the FRACMAN code to generate a statistical fracture system that represented the NGDFA. Ten stochastic DFN realizations were generated, and the fracture characteristics of the simulated fracture systems then were compared to the DLS field data from the NGDFA. When the stochastically generated

Table 14. Statistical summary of porosity values from the type-curve analytical solutions of cross-hole air-injection testing of the northern Ghost Dance Fault

[m^3/m^3, cubic meter per cubic meter]

Structural unit	Arithmetic mean (m^3/m^3)	Arithmetic range (m^3/m^3)	Geometric mean (m^3/m^3)
Hanging wall	0.04	0.01-0.09	0.03
Fault zone	0.13	0.05-0.27	0.10
Footwall	0.04	0.01-0.12	0.03

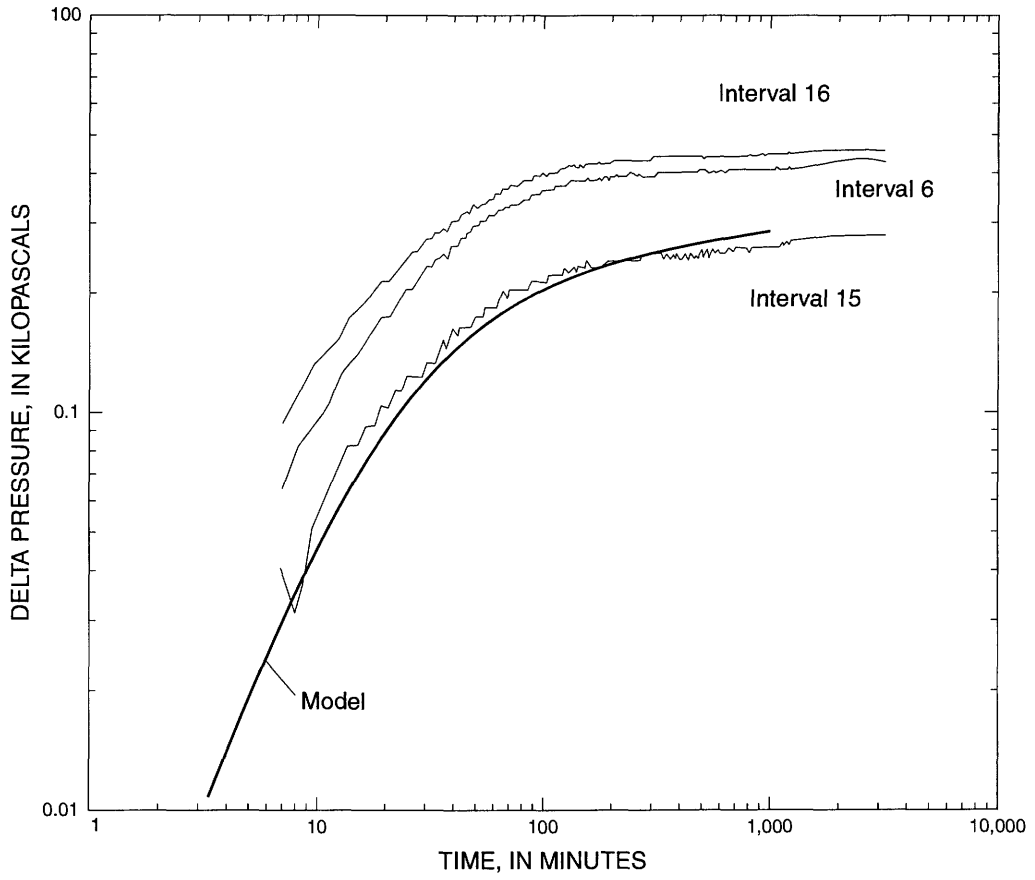

Figure 13. Pressure, with time, measured during air-injection test 16 for monitor intervals 6, 15, and 16 located at 4.4, 4.5, and 4.1 meters from the injection interval, and the numerical model predicted pressure response at a distance of 4.5 meters from the injection interval.

DFN fracture data were within one standard deviation of the DLS field data, the DFN model was calibrated. The input parameters for the six fracture sets used to generate the DFN model are listed in table 15. An additional three fracture sets that were applied to the intensely fractured 4-meter-wide fault zone are listed in table 16. The additional three fracture sets are based on a visual inspection of the fault zone and were included to compensate for the high density of fractures with trace lengths less than 0.3 m that were not included in the DLS.

Following the development of the fracture system, transmissivity values were assigned to the fractures. The initial transmissivity values were derived from the permeability values from the type-curve analysis of the cross-hole air-injection tests. The transmissivity distributions and the equivalent permeability values for the FRACMAN-DFN model footwall, fault zone, and hanging wall that best matched the cross-hole pneumatic field-testing data are listed in table 17. The transmissivity values are based on an interval length of 2 m.

The permeability values from the DFN model are larger but generally in close agreement with the permeability values from the type curve and the AIR3D analysis. The steady-state pressure responses from cross-hole air-injection test 25 and the simulated steady-state pressure responses from the DFN model are presented in figure 14. The injection interval for test 25 and monitor intervals 1, 2, 3, 4, 5, 11, 12, 13, and 14 were located in the hanging wall of the GDF. Monitor intervals 6, 7, 15, and 16 were located in the fault zone and monitor intervals 8, 9, 10, 17, 18, 19, and 20 were located in the footwall. The simulated pressure responses from the DFN model were similar to the field-testing pressure responses and indicated that the DFN model had replicated the fracture network and fracture permeability of the hanging wall. The steady-state pressure responses from the cross-

Table 15. Input parameters of the six fracture sets used to produce the FRACMAN discrete-features model

[--, not applicable; k, permeability; SD, standard deviation; m^2/m^3, square meter per cubic meter]

Fracture set	Orientation						Size			
	Model type	Strike/dip (degrees)	Pole orientation trend/plunge (degrees)	Distribution type	Dispersion (k)	Equivalent radius (meters)	Distribution type	Mean / SD (meters)	Max / Min (meters)	Intensity (m^2/m^3)
1	Baecher	059/88	329/02	Fisher	50	--	Truncated log-normal	0.614/0.27	0.3/150.0	0.17
2	Baecher	075/84	345/06	Fisher	35	--	Truncated log-normal	0.62/1.8	0.3/150.0	0.22
3	Baecher	125/84	035/06	Fisher	25	--	Truncated log-normal	0.97/2.06	0.3/150.0	2.07
4	Baecher	332/63	242/27	Fisher	25	--	Truncated log-normal	0.56/0.8	0.3/150.0	0.08
5	Baecher	192/87	099/03	Fisher	36	0.277	Truncated power law	2.5	0.3/150/0	2.56
6	Baecher	199/63	109/27	Fisher	20	--	Truncated exponential	0.54	0.3/150.0	0.11

Table 16. Input parameters of the three additional fracture sets used in the fault zone to produce the FRACMAN discrete-features model

[--, not applicable; k, permeability; SD, standard deviation; m^2/m^3, square meter per cubic meter]

Fracture set	Orientation						Size			
	Model type	Strike/dip (degrees)	Pole orientation trend/plunge (degrees)	Distribution type	Dispersion (k)	Equivalent radius (meters)	Distribution type	Mean / SD (meters)	Max / Min (meters)	Intensity (m^2/m^3)
1	War zone	035/90	125/00	Fisher	50	--	Truncated log-normal	0.5/1.0	0.1/2.0	0.0002
2	War zone	000/90	090/00	Fisher	50	--	Truncated log-normal	0.5/1.0	0.1/2.0	0.0002
3	War zone	315/90	045/00	Fisher	50	--	Truncated log-normal	0.5/1.0	0.1/2.0	0.0002

Table 17. Transmissivity distributions and equivalent permeability values for the discrete-feature model

[m^2/s, meter squared per second]

Structural unit	Distribution type	Transmissivity mean (m^2/s)	Transmissivity standard deviation (m^2/s)	Permeability mean (m^2)
Footwall	Log-normal	9.06×10^{-04}	2.30×10^{-04}	45.3×10^{-12}
Fault zone	Log-normal	9.06×10^{-04}	2.30×10^{-04}	45.3×10^{-12}
Hanging wall	Log-normal	2.31×10^{-04}	8.30×10^{-04}	11.6×10^{-12}

hole air-injection test 36, and the DFN model-simulated steady-state pressure responses are presented in figure 15. The injection interval for test 36 was located in the footwall of the GDF. The monitor intervals were the same as in test 25. The simulated pressure responses were similar to the field pressure responses and indicated that the DFN model had replicated the fracture network and the fracture permeability of the footwall. The steady-state pressure responses from the cross-hole air-injection test 32 and the DFN model-simulated steady-state pressure responses are presented in figure 16. The injection interval for test 32 was in the fault zone. The monitor intervals were the same as in tests 25 and 36. The simulated pressure responses from the DFN model were generally higher than the field pressure responses by a factor of 3. To correct this discrepancy, the fracture intensity and transmissivity values for the DFN fault zone were increased as much as an order of magnitude. However, the changes did not have a substantial effect on the simulated pressure responses. A dual-porosity model was run to determine if matrix porosity, associated with the breccia located in the fault zone, had any effect on the simulated pressure responses; the simulated pressure responses decreased slightly but did not change substantially. Only matrix porosity values of 50 percent decreased the DFN model-simulated pressure responses to field-test values. Although core

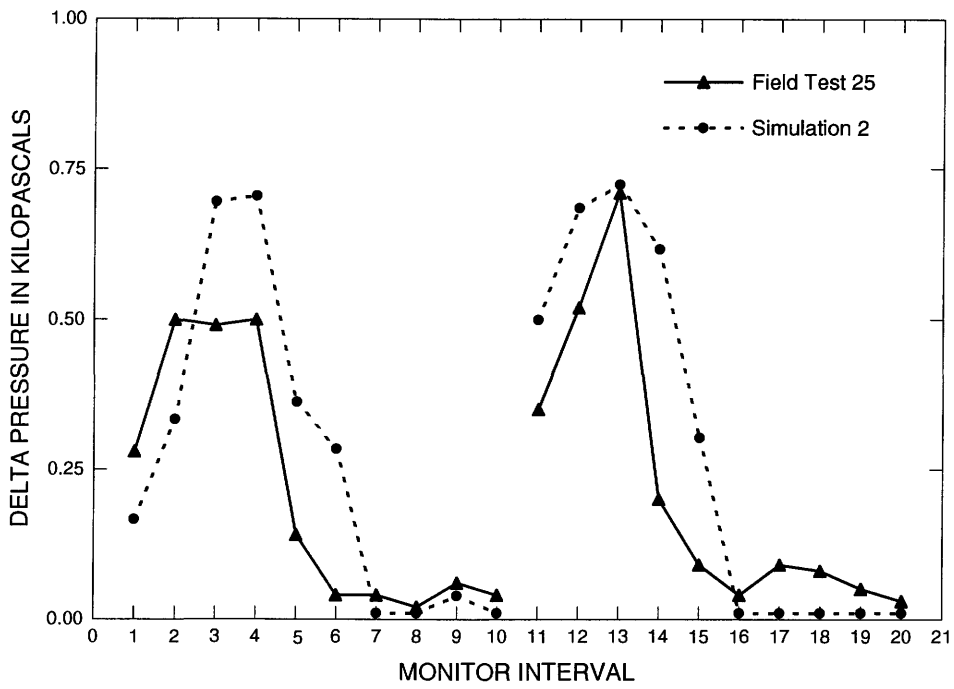

Figure 14. Pressure changes measured during cross-hole air-injection test 25 and the pressure changes simulated by the discrete-feature model.

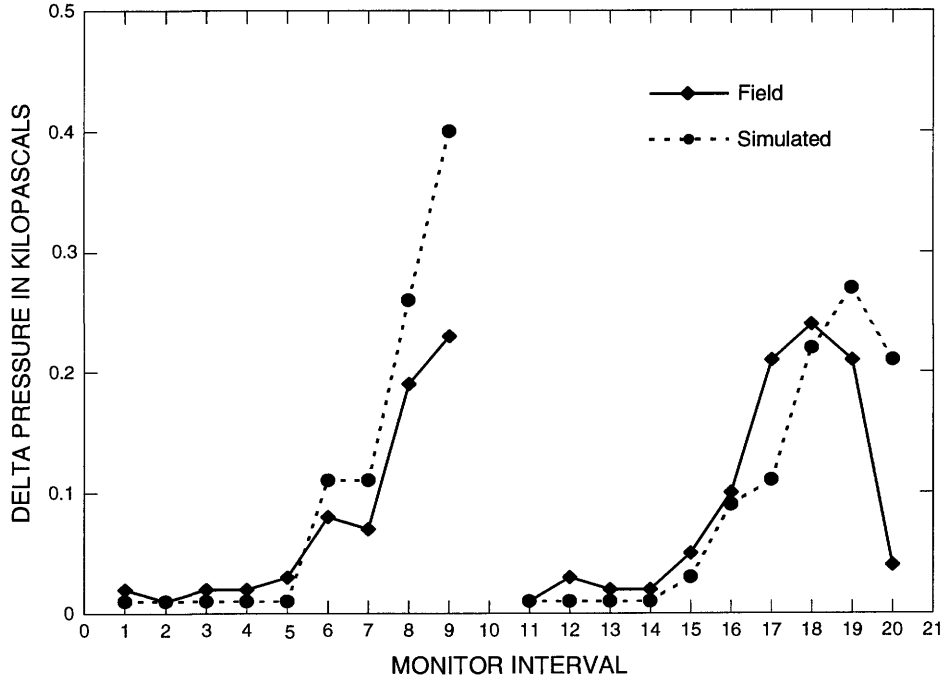

Figure 15. Pressure changes measured during cross-hole air-injection test 36 and the pressure changes simulated by the discrete-feature model.

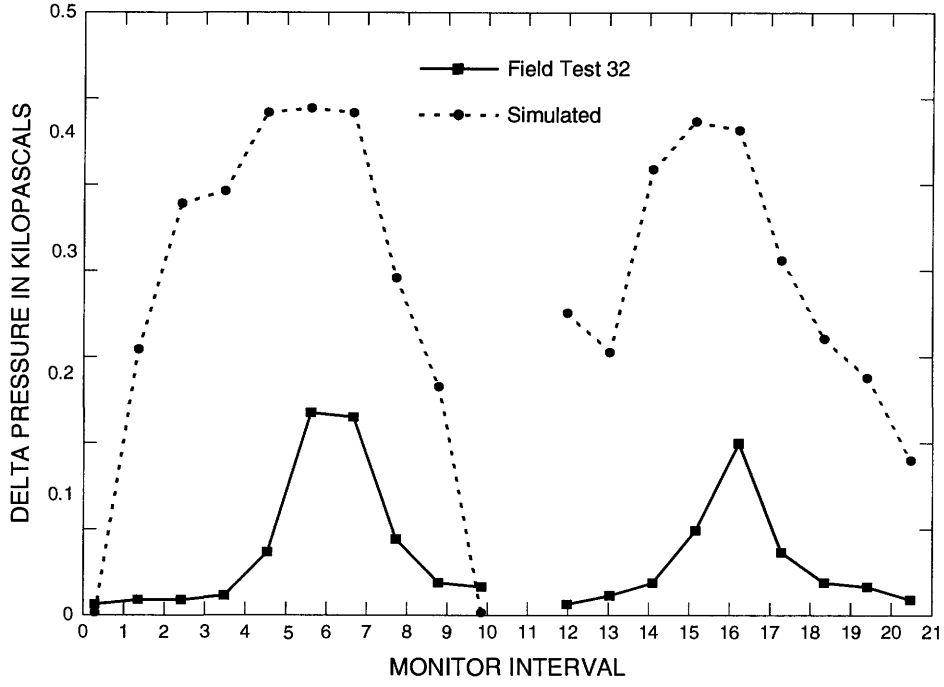

Figure 16. Pressure changes measured during cross-hole air-injection test 32 and the pressure changes simulated by the discrete-feature model.

analysis from borehole MF#3 indicated rubble zones and dense fracturing in the fault zone, a 50-percent air-filled porosity was considered too large to be realistic.

The DFN model indicated that cross-hole air-injection tests done in the GDF hanging wall and footwall can be simulated accurately using the DLS fracture-mapping data; and, because the model is based on real fracture data, the DFN will produce a more realistic fracture-flow model. The DFN model of the fault zone was not as successful because the intense fracturing of the fault zone was not adequately represented in the DLS fracture data. The DLS fracture mapping was limited to fractures with trace lengths greater than 0.3 m; most of the fractures in the fault zone, although numerous, had trace lengths less than 0.3 m and were not mapped nor were they adequately represented by the three additional fracture sets. The AIR3D numerical modeling indicated that, due to the high fracture density, the fracture zone is probably better simulated as an equivalent porous medium. Because the DFN provides a model of the footwall and hanging wall that is closer to reality, it may be possible to increase the scale of the DFN simulations to predict pressure responses at larger dimensions for areas that have fracture systems similar to the GDF hanging wall and footwall.

Results from Cross-Hole Tracer Testing in the Northern Drill Room Boreholes

Analysis Using Type Curves

The cross-hole tracer tests were analyzed using type curves (Moench, 1995). The results of the tracer-test type-curve analysis are listed in table 18. Several tracer tests were unsuccessful because of equipment failure or other unforeseen problems. A plot of a typical tracer test and type-curve match is presented in figure 17. Peclet numbers ranged from 3 to 22 except for a single test that resulted in two Peclet numbers of 80 (table 18). Advective traveltimes ranged from 0.011 to 1.110 days. Transport-porosity values ranged from 0.001 to 0.070. Longitudinal-dispersivity values ranged from 0.06 m to 2.63 m. Tracer tests 1 through 8 generally had similar tracer arrival plots for He and SF_6. The similar plots indicated that the small He molecule did not diffuse more readily into the small matrix pores and that the larger SF_6 molecule was not adsorbed onto tuff materials as it has been shown to do (Rattray and others, 1995); or, the effects are small and of the same order of magnitude.

A statistical summary of the northern GDF transport-porosity and longitudinal-dispersivity values by geologic structure are listed in table 19. Tracer tests done in the footwall of the GDF had transport-porosity values that ranged from 0.003 to 0.032 with an average value of 0.013. Tracer tests done in the fault zone had transport-porosity values that ranged from 0.004 to 0.034 with an average value of 0.014. Tracer tests done in the hanging wall had transport-porosity values that ranged from 0.001 to 0.070 with an average value of 0.013. Tracer tests done in the footwall of the GDF had longitudinal-dispersivity values that ranged from 0.42 to 1.54 m with an average of 1.03 m. Tests done in the fault zone had longitudinal-dispersivity values that ranged from 0.37 to 1.38 m with an average of 0.62 m. Tests done in the hanging wall had longitudinal-dispersivity values that ranged from 0.06 to 2.63 m with an average of 0.76 m.

The wide range of transport-porosity and longitudinal-dispersivity values may indicate that the test scale was smaller than the representative elementary volume. Figure 18 is a lower hemisphere plot showing the direction and plunge of the tracer tests and the calculated transport-porosity values. The plot does not indicate any directional control; slow and fast tracer transport pathways occur in the same direction and plunge. The tracer data and locations of the pumped and tracer release intervals for the individual cross-hole tracer tests are available in the YMP data packages DTN: GS980283122410.003 and GS981183122410.005.

A plot of the longitudinal-dispersivity values with test scale for several NTS fractured-rock tracer test programs, including the NGDFA tracer testing, is shown in figure 19. The plot indicated that the longitudinal-dispersivity values increase with test scale. The data for the Amargosa Tracer site are from Gelhar and others (1992) and the C-wells data are from Fahy (1997).

Discrete-Feature Analysis Using MAFIC

The MAFIC computer code (Miller and others, 1994) was used to simulate tracer flow in the DFN model developed using FRACMAN. The MAFIC code uses a three-dimensional network of triangular finite elements for either a single- or a dual-porosity mode. The MAFIC code simulates solute transport

Table 18. Results of tracer-test analysis by type curves

[He, helium; SF_6, sulfur hexafluoride; --, no data; m^3/m^3, cubic meter per cubic meter]

Test number and tracer	Structural unit	Linear distance (meters)	Advective traveltime (days)	Peclet number	Longitudinal dispersivity (meters)	Transport porosity (m^3/m^3)
1He	Footwall	4.81	0.212	8	0.60	0.019
$1SF_6$	Footwall	4.81	0.235	6	0.80	0.032
2He	Fault zone	4.78	0.153	11	0.43	0.014
$2SF_6$	Fault zone	4.78	0.130	8	0.60	0.012
3He	Hanging wall	4.78	0.032	80	0.06	0.002
$3SF_6$	Hanging wall	4.78	0.032	80	0.06	0.002
4He	Hanging wall	5.48	0.366	12	0.46	0.018
$4SF_6$	Hanging wall	5.48	--	--	--	--
5He	Hanging wall	6.02	0.162	9	0.67	0.005
$5SF_6$	Hanging wall	6.02	0.129	9	0.67	0.004
6He	Hanging wall	5.29	0.600	11	0.48	0.030
$6SF_6$	Hanging wall	5.29	0.575	5	1.06	0.029
7He	Footwall	4.61	0.028	3	1.54	0.003
$7SF_6$	Footwall	4.61	0.028	3	1.54	0.003
8He	Footwall	4.57	0.218	3	0.91	0.023
$8SF_6$	Footwall	4.57	--	--	--	--
9He	Hanging wall	6.37	0.580	9	0.71	0.018
$9SF_6$	Hanging wall	6.30	0.570	--	--	0.018
10He	Hanging wall	4.97	0.077	6	0.83	0.005
$10SF_6$	Hanging wall	6.04	0.083	22	0.27	0.003
11He	Hanging wall	7.90	1.110	3	2.63	0.015
$11SF_6$	Hanging wall	8.78	0.334	22	0.40	0.003
12He	Hanging wall	5.06	0.137	5	1.01	0.070
$12SF_6$	Hanging wall	4.32	0.208	11	0.39	0.017
13He	Footwall	4.23	0.251	3	1.41	0.003
$13SF_6$	Footwall	4.65	0.066	11	0.42	0.005
14He	Footwall	6.60	--	--	--	--
$14SF_6$	Footwall	6.52	--	--	--	--
15He	Fault zone	4.88	0.453	11	0.44	0.034
$15SF_6$	Fault zone	4.13	0.142	11	0.37	0.018
16He	Fault zone	6.89	0.433	5	1.38	0.011
$16SF_6$	Fault zone	5.39	--	--	--	--
17He	Hanging wall	7.03	0.195	8	0.88	0.004
$17SF_6$	Hanging wall	5.38	0.100	5	1.08	0.005
$17SF_6$	Hanging wall	5.38	0.159	11	0.49	0.008
14He	Hanging wall	6.53	0.219	6	1.09	0.006
$14SF_6$	Hanging wall	8.75	--	--	--	--
15He	Fault zone	4.30	0.050	8	0.54	0.004
$15SF_6$	Fault zone	5.19	--	--	--	--
16He	Fault zone	5.02	0.092	9	0.56	0.006
$16SF_6$	Fault zone	5.25	--	--	--	--
17He	Hanging wall	4.21	0.172	5	0.84	0.019
$17SF_6$	Hanging wall	5.04	0.060	5	1.01	0.004
$17SF_6$	Hanging wall	5.04	0.011	22	0.23	0.001

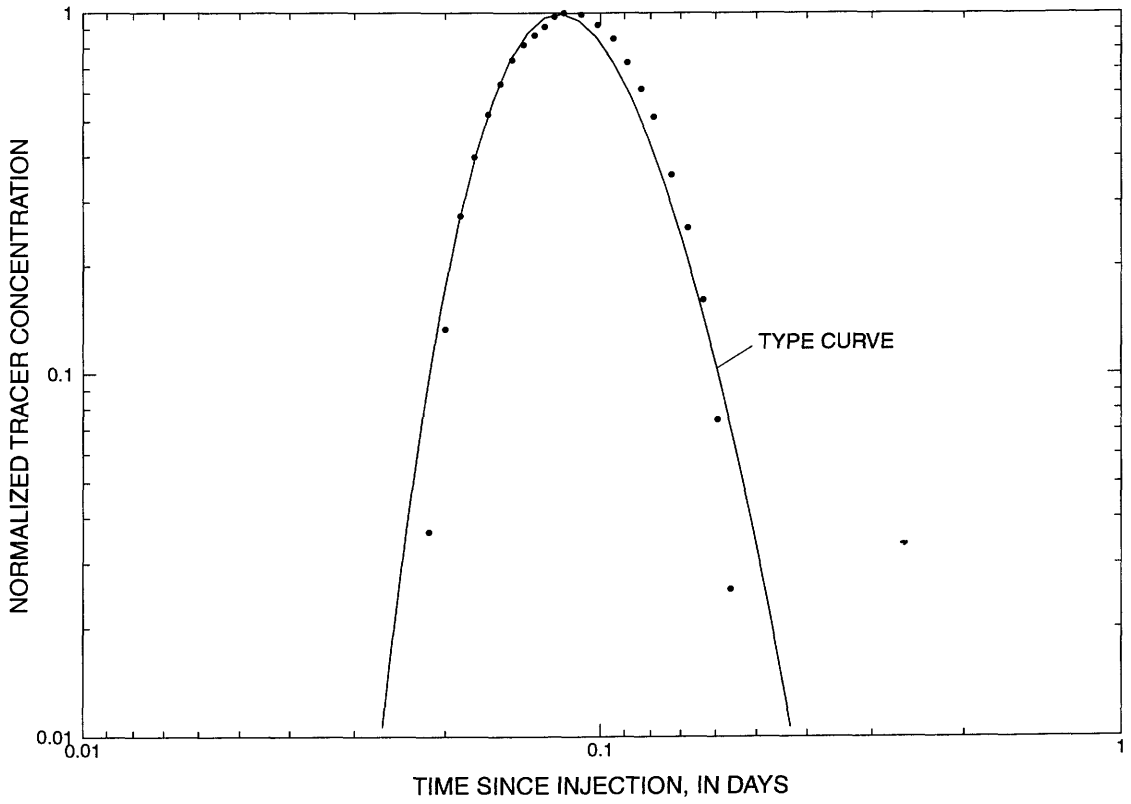

Figure 17. Sulfur hexafluoride tracer arrival plot during tracer test 10 and type curve match.

using an advective particle-tracking approach. Solute dispersion was simulated stochastically using orthogonal, normally distributed, longitudinal and transverse dispersion vectors. Because of the small scale (<10 m) and the short transport times (<200 minutes) diffusion was assumed to be negligible. The DFN-MAFIC model was set up to model the SF_6 convergent-tracer tests 15, 17, and 21. The simulations used the same pumping rates used in the field testing, about 5.0×10^{-04} m^3/s (30.0 sLpm) and a fluid viscosity of 1.8×10^{-5} Pa × s. The MAFIC code limits the number of tracer particles to less than 1,000; therefore, the number of tracer particles ranged from 927 to 995. The simulations used a longitudinal-dispersivity value of 1.0 m, derived from the type-curve analysis, and assumed that the transverse dispersivity was 10 percent of the longitudinal value (0.1 m).

A normalized simulated-tracer-arrival curve and the normalized field data from tracer test 17 are presented in figure 20. Background SF_6 concentrations during tracer tests 15, 17, and 21 were low, generally less than 0.1 ppm with a maximum of less than

Table 19. Statistical summary of the northern Ghost Dance Fault transport-porosity and longitudinal-dispersivity values by geologic structure

[m^3/m^3, cubic per cubic meter; arithmetic mean in parentheses]

Geologic structure	Transport-porosity range (m^3/m^3)	Longitudinal-dispersivity range (meters)
Footwall	0.003-0.032 (0.013)	0.42 - 1.54 (1.03)
Fault zone	0.004-0.034 (0.014)	0.37 - 1.38 (0.62)
Hanging wall	0.001-0.070 (0.013)	0.06 - 2.63 (0.76)

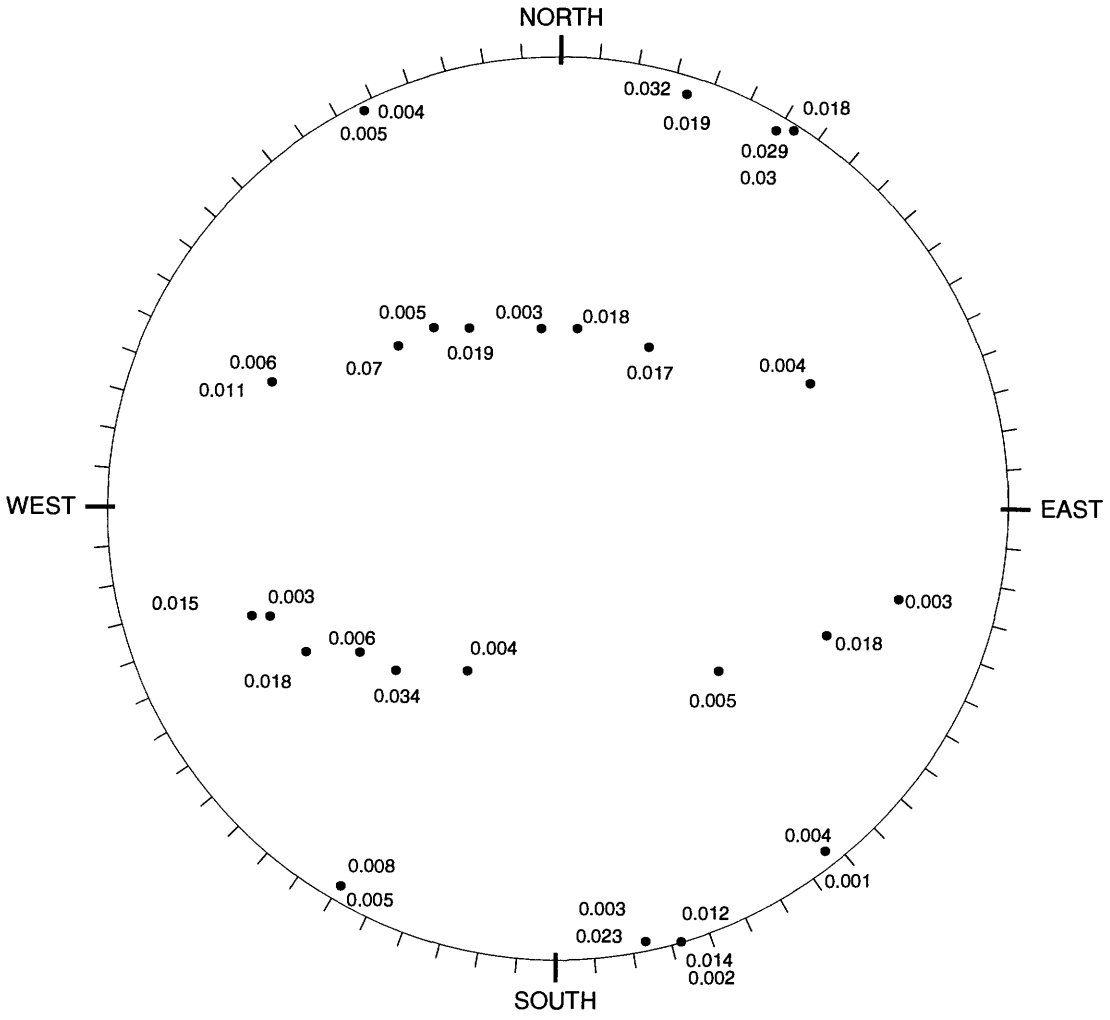

Figure 18. Stereonet plot showing a lower hemisphere plot of transport-porosity values and the three-dimensional orientation, by bearing and plunge, of the associated tracer tests.

1.0 ppm, and therefore were not compensated for in the analysis. During tracer test 17, the SF_6 tracer-release interval and the pumped interval were located in the hanging wall. The peak arrival time was 200 minutes. The early-time simulated values were a close match to the field data except for the simulated values near 60 to 80 minutes. The spikes in the simulated curve may be because of the limited number of tracer particles or because there was not a sufficient number of time steps to smooth the curve. Generally, the simulated tracer arrival was a close match to the field data; therefore, the DFN model had replicated the fracture flow and transport in the GDF hanging wall.

A normalized simulated-tracer-arrival curve and the normalized field data from tracer test 21 are presented in figure 21. During tracer test 21, the SF_6 tracer-release interval and the pumped interval were located in the footwall. The simulated peak-arrival time was 55 minutes. The peak arrival time during the field test was 95 minutes. The shapes of the two curves are similar, including curve spreading and tailing; first and last arrival times also are similar. The spikes in the simulated curve may be because of the limited number of tracer particles or because the number of time steps was insufficient to smooth the curve. The 40-minute difference between peak arrival times may indicate that the simulated fractures have better connections from source (tracer release interval) to sink (pumped interval) than the true fracture network. Although the peak-arrival times are different, the DFN model

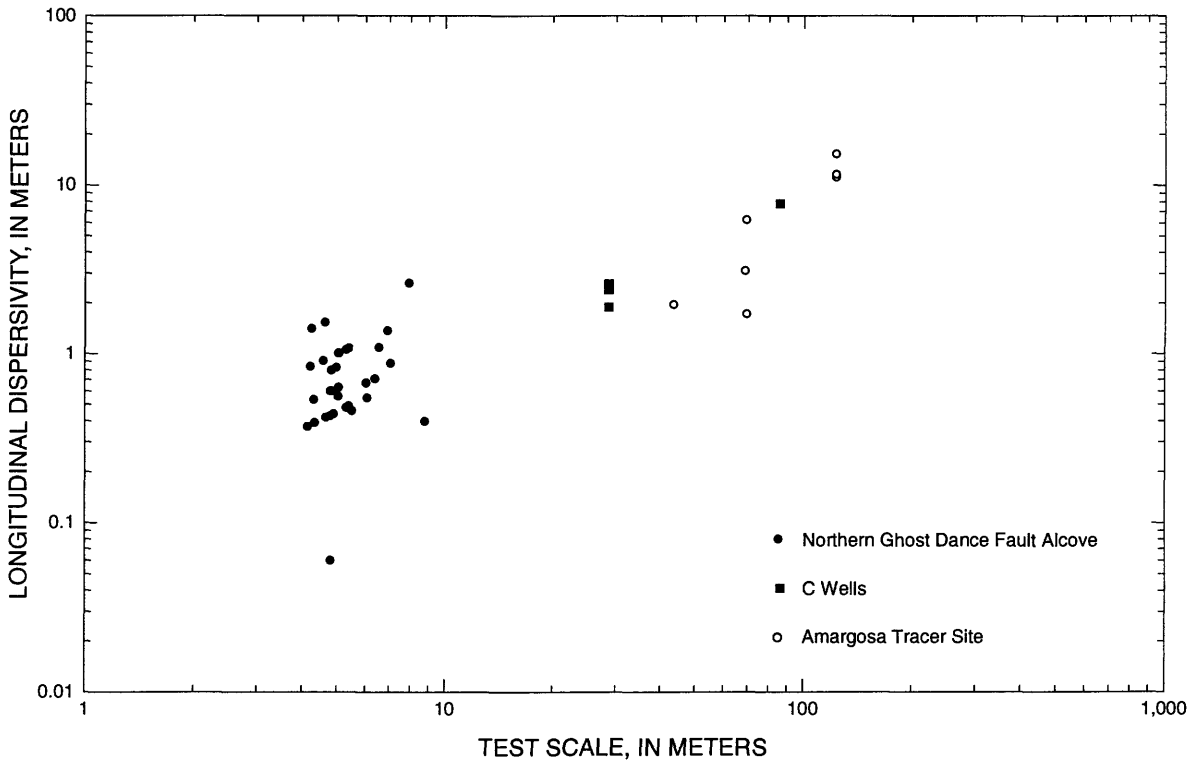

Figure 19. Longitudinal-dispersivity values and test scale for tracer tests performed at or near Yucca Mountain.

provides a more realistic numerical understanding of fracture flow and transport in the footwall than the equivalent continuum approach.

The traveltimes measured during the fault-zone tracer testing did not indicate that the transport porosity of the fault zone was higher than the footwall nor the hanging wall, despite the increased fracturing in the fault zone. A normalized simulated-tracer-arrival curve and the normalized field data from test 15 are presented in figure 22. During tracer test 15, the SF_6 tracer-release interval and the pumped interval were located in the fault zone. The simulated tracer test was not a close match to the field data. The peak-arrival time for the simulated test was 50 minutes. The peak-arrival time of test 15 was 190 minutes. A dual-porosity model was run to determine if an increase in the total porosity would produce a peak-arrival time that was more consistent with the field data. Simulated tracer-arrival times that approached the field-arrival times were accomplished only when matrix porosities were increased to 50 percent. Although core analysis from borehole MF#3 indicated rubble zones and dense fracturing in the fault zone, a 50-percent air-filled porosity was considered too large to be realistic. Representative fracture geometry is difficult to extract from these broken zones and the fault-zone intense fracturing was not captured in the DLS. As was concluded from the cross-hole air-injection testing analysis, the DFN model did not adequately represent the fault-zone fracture system.

The flow paths of two particles during the DFN simulation of tracer test 17 are presented in figure 23. A particle tracker was used to visualize the flow path from the source (tracer-release interval) to the sink (pumped interval). The tracking indicated that the particles followed a tortuous and indirect route. The flow paths indicated that the travel distances of the tracked particles were up to six times longer than the linear distance. The long, tortuous flow paths are a partial explanation for the high transport-porosity values (up to 0.070) compared to the true fracture porosity that usually ranges between 10^{-2} to 10^{-5} (Freeze and Cherry, 1979, p. 408). The variability in the length of the flow paths also indicated that a drawn-out arrival-time tail may not necessarily be a result of matrix diffusion but could be a result of a complex, variable, nonlinear tracer-transport route.

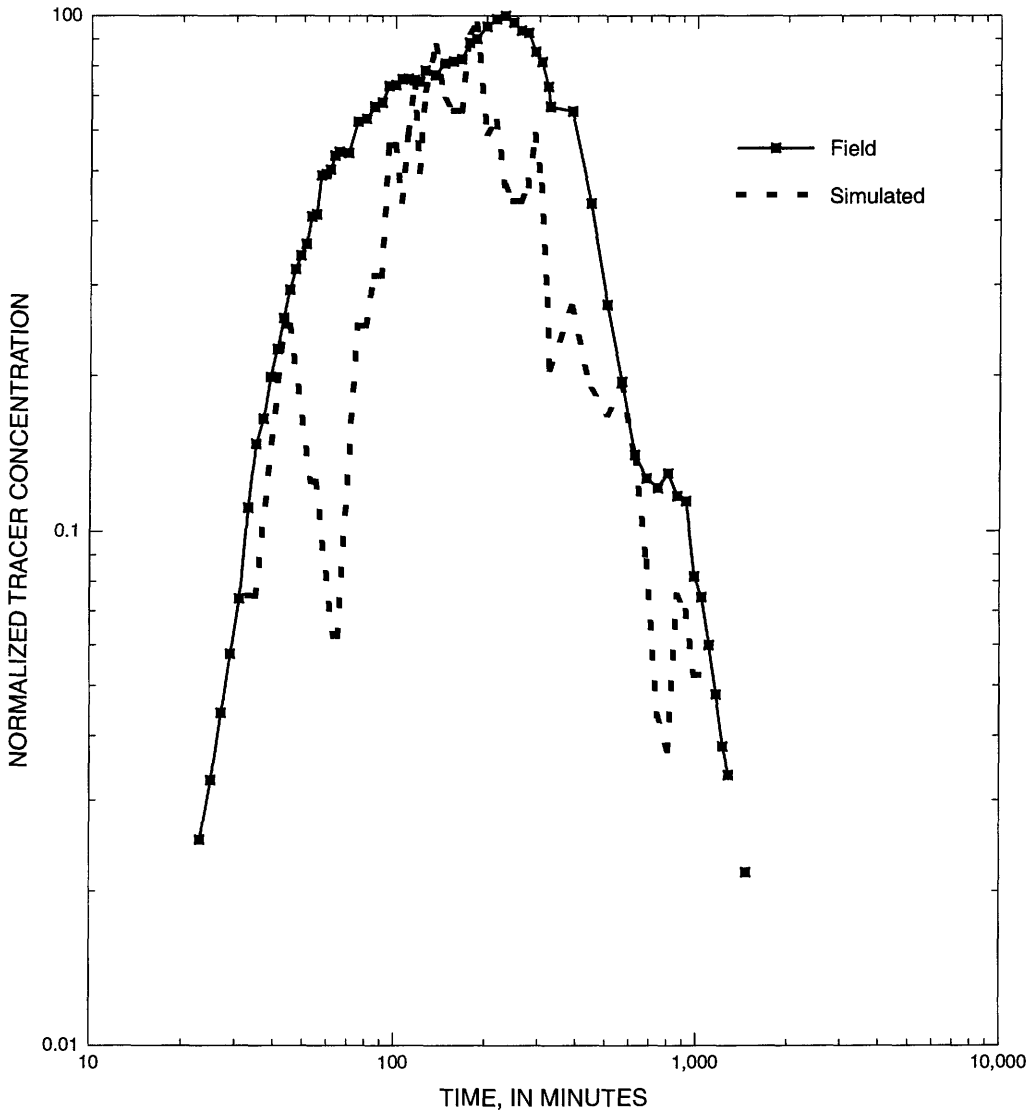

Figure 20. Tracer-arrival plot for tracer test 17 SF_6 and tracer-arrival plot predicted by the discrete-feature model.

The DFN model indicated that tracer tests done in the GDF hanging wall and footwall can be accurately simulated using data from DLS fracture mapping; and, because the DFN model is based on real fracture data, the DFN approach results in a more realistic transport model. The DFN model of the GDF fault zone was not as successful because the intense fracturing was not adequately represented by the DLS fracture data and therefore was not adequately represented in the model. The DLS fracture mapping was limited to fractures with trace lengths greater than 0.3 m; most of the fractures in the fault zone, although numerous, had trace lengths less than 0.3 m. The DFN modeling indicated that, due to the high fracture density, the fracture zone is probably better modeled as an equivalent porous medium. Because the DFN model is based on real fracture data, it provides a more accurate model of the footwall and hanging wall fracture-flow system, as opposed to the equivalent porous-medium approach. Because the DFN model provides a model that is closer to reality, it may be possible to increase the scale of the DFN simulations to predict transport at larger dimensions for areas that have fracture systems similar to the fracture systems of the GDF footwall and hanging wall.

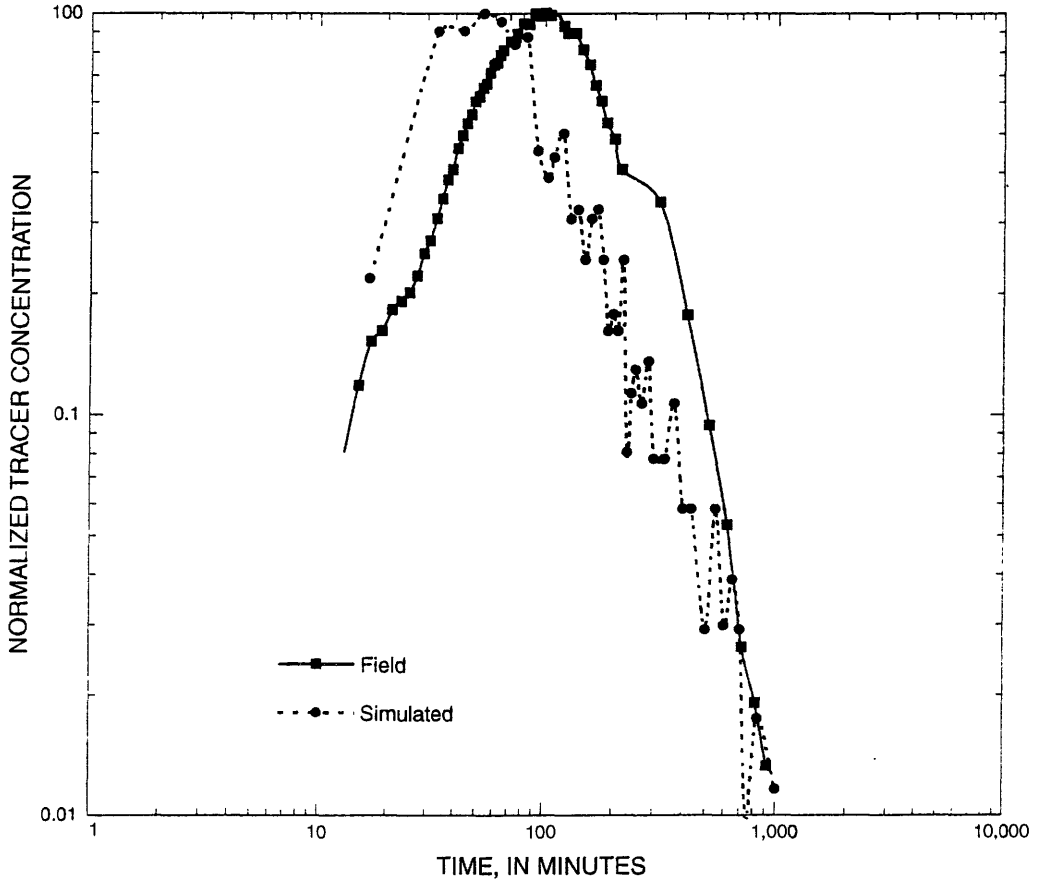

Figure 21. Tracer-arrival plot for tracer test 21 SF_6 and tracer-arrival plot predicted by the discrete-feature model.

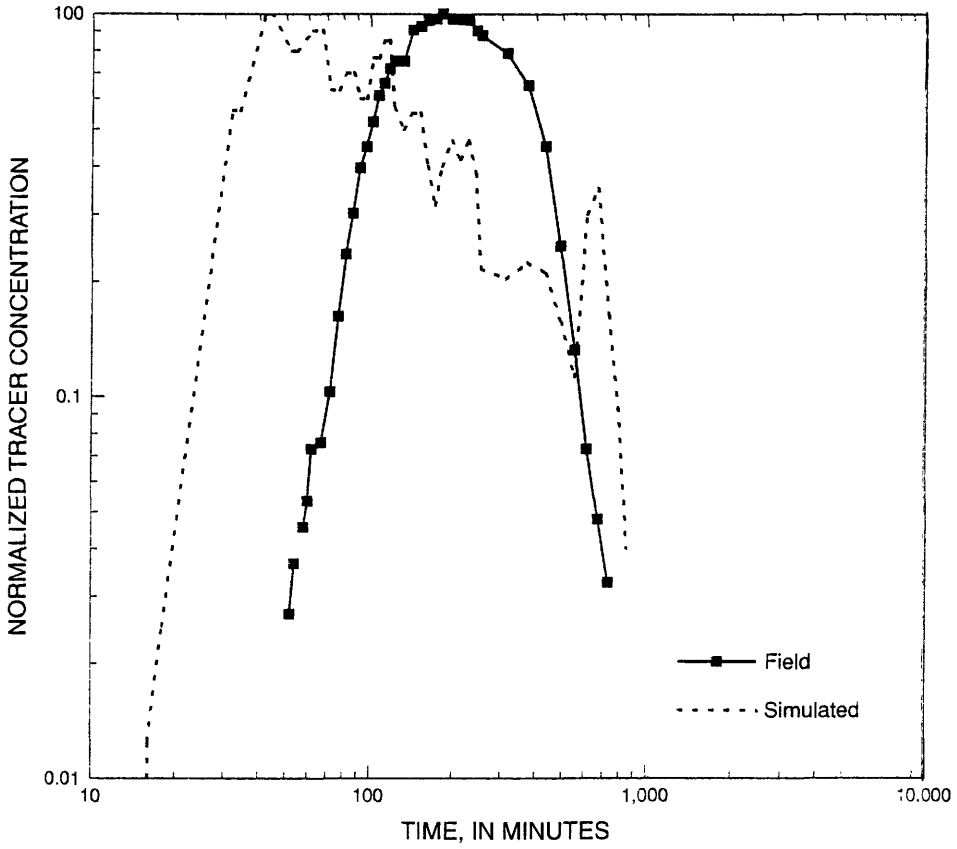

Figure 22. Tracer-arrival plot for tracer test 15 SF_6 and tracer-arrival plot predicted by the discrete-feature model.

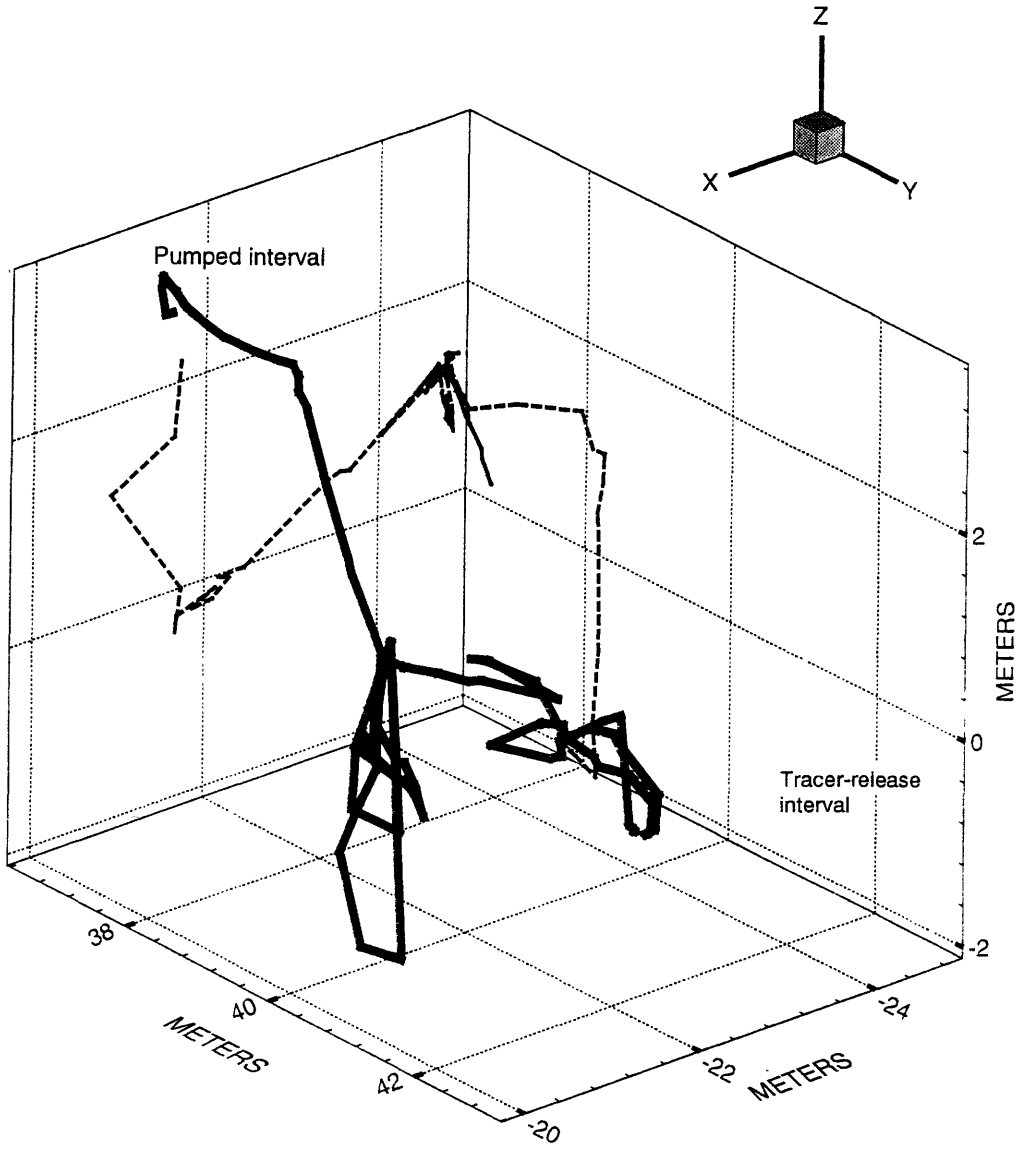

Figure 23. Diagram showing particle paths predicted by the discrete-feature model for two particles.

SUMMARY

Geothermal logging, air and core-water chemistry sampling, air-injection testing, and tracer testing were done in the northern Ghost Dance Fault (GDF) at Yucca Mountain, Nevada. The goals of the fault testing were to quantify the permeability values, porosity values, tracer-transport characteristics (transport porosity, longitudinal dispersivity), and fluid ages of the GDF and the volcanic rocks (tuff) of the footwall and hanging wall. The GDF testing was part of the Yucca Mountain Project (YMP) scientific study done by the U.S. Geological Survey in cooperation with the Department of Energy (DOE) to evaluate the potential for geologic disposal of high-level radioactive waste in an unsaturated-zone desert environment.

The Northern Ghost Dance Fault Alcove (NGDFA) consists of two sections—the Northern Ghost Dance Fault Access Drift (NAD) and the Northern Ghost Dance Fault Drill Room (NDR). The NAD is located 3,737 m into the Exploratory Studies Facility (ESF) (measured from the ESF north entrance) and is about 230 m below the land surface. The NAD was constructed at a heading of due east and was initially constructed to a depth of 105 m (measured from the ESF centerline). From the face of the NAD, borehole NAD-GTB#1a was drilled horizontally, at a heading of due east to a depth of 60 m. Borehole NAD-GTB#1a penetrated the GDF at a depth of approximately 49 m. A downhole video log was run on November 1, 1996, and a geothermal log was run on November 7, 1996. After the geothermal logging was completed, excavation of the NAD was continued to a depth of 134.4 m, eliminating the upper 29.4 m of borehole NAD-GTB#1a. Following the construction, geothermal logging, air-injection testing, and chemistry sampling were done in the remaining section of borehole NAD-GTB#1a. After the testing was completed, construction of the NAD continued to a depth of 174 m. The NAD intersected the main trace of the GDF at 152 m. Following completion of the NAD, the NDR was excavated at a heading of due north to a depth of 24 m. Following construction of the NDR, three test boreholes were drilled from the NDR into the GDF. The boreholes had western headings, were near horizontal, were parallel, were 30.5, 30.6, and 34.4 m in depth, and were oriented in a triangular configuration with 4.2-m sides.

The NGDFA and the boreholes are in the crystal-poor, middle nonlithophysal zone of the Topopah Spring Tuff (Tptpmn). Borehole NAD-GTB#1a was drilled from the hanging wall of the GDF, through the fault and into the footwall. The initial geologic interpretations of the fault and the broken zone (zone of intense fracturing) were based on the video log from borehole NAD-GTB#1a. The video log identified a 12-m-wide broken zone that was variably brecciated, and consisted of fractured rock that had matrix- and clast-supported breccia zones. Excavation through the GDF revealed no distinct planes along the hanging wall and footwall and no slickensides. The GDF is a normal fault with a strike/dip of 180/80 on the footwall and 175/82 on the hanging wall. The fault offset is approximately 3 meters. No secondary calcite or silica/opal was visible in the breccia or surrounding rock. Downhole video and caliper logs done in boreholes MF#1, MF32, and MF#3 identified an intensely fractured zone that extended from the main trace of the GDF about 1 m into the footwall and 3 m into the hanging wall. The intensely fractured zone is herein referred to as the "fault zone."

The geothermal log from borehole NAD-GTB#1a indicated penetration of the NGDFA ventilation to depths of 3 to 5 m and a 0.1°C temperature decrease throughout the 12-m-wide broken zone. The temperature decrease could indicate movement of cool air or water, or both, down the 12-m-wide broken zone. A geothermal log done at a later date did not record the previously measured temperature drop across the 12-m-wide broken zone but identified a 0.05°C temperature increase at or near the main trace of the GDF. The temperature increase may indicate deep, warm air moving up the main trace of GDF. The stabilization of the temperature of the 12-m-wide broken zone may indicate that the earlier measured temperature drop may have been due to drilling-induced evaporative cooling or gas-expansion adiabatic cooling. Other temperature fluctuations may be due to drilling effects or possibly due to the variable borehole diameter. A more thorough understanding of the effect of barometric pressure on the temperature in the fault and 12-m-wide broken zone requires that geothermal logs be done during a range of barometric pressure fluctuations.

In-situ pneumatic pressures monitored in borehole NAD-GTB#1a indicated limited barometric attenuation and small time lags. Comparison of the downhole-monitor interval pressure fluctuations (0.56 to 0.83 kPa) to the barometric-pressure fluctua-

tion (1.07 kPa) indicated that the permeability of the rock is high. Pressure monitoring showed no correlation between the amount of pressure attenuation and the distance from the NAD and no correlation between pressure attenuation and the distance from the main trace of the GDF. The amount of attenuation shows no pattern and may be random. The intermediate attenuation measured in monitor port 10, located farthest from the NAD, may indicate that the barometric pressure changes were transmitted from the land surface to depth through the GDF.

Gas-phase chemistry samples were collected in borehole NAD-GTB#1a. The gas-phase CO_2 concentrations ranged from 660 to 1,175 ppm. The CO_2 values increased and the $\delta^{13}C$ values decreased with increasing distance from the NAD ($r = 0.89$, and $r = 0.84$). The CO_2 and $\delta^{13}C$ values indicated that air from the NAD has penetrated the tuff, supporting the concept of a well-developed fracture connection to the NAD. Uncorrected ^{14}C-age estimates from gas-samples ranged from 2,400 to 4,500 years. The ^{14}C-ages from the monitor intervals are directly correlated ($r = 0.75$) to the degree of pressure attenuation that was measured during pneumatic monitoring. The age/attenuation correlation indicated that air from the NAD had penetrated the tuff through the fracture system. Tritium analysis (classified as non-quality assured) on core water identified eight samples at six depths that had tritium levels significant at two standard deviations. Three of the samples, at two depths, indicated that water had traveled from the land surface to depth during the last 45 years. The proximity of the elevated tritium values to the main trace of the GDF indicated that the fault is a conduit for the transport of water from the land surface through the nonwelded tuff of the Paintbrush Group and down to the Tptpmn.

Gas-phase chemistry samples were collected in boreholes MF#1 and MF#2. The gas-phase CO_2, concentrations ranged from 711 to 913 ppm. Gas-phase $\delta^{13}C$ values ranged from -15.04 to -13.45. Gas-phase ^{14}C ages ranged from 2,500 to 3,600 years. There was no correlation between the parameters and depth. The data indicated that the gas samples were a mixture of NGDFA air and rock gas. A gas-sample from a monitor interval in the fault zone had the lowest CO_2, largest $\delta^{13}C$, and youngest ^{14}C age, all indicating mixing with the NGDFA air. The mixing is probably due to (1) the high permeability of the fault zone, as identified in the air-injection testing; (2) the NAD penetration of the GDF, providing a short flow path; and (3) the 17 months that elapsed between the NAD fault penetration in March 1997 and the gas sampling in August 1998. Tritium analysis (classified as non-quality assured) of core water from the two samples from borehole MF#1 had tritium levels significant at two standard deviations. The NDR borehole tritium data indicated that the fault is a conduit for the rapid transport (< 100 years) of water from the land surface through the nonwelded tuff of the Paintbrush Group and down to the Tptpmn, assuming that the tritium levels are not due to contamination.

Single-hole air-injection testing was done in borehole NAD-GTB#1a. The permeability values of the hanging wall ranged from 0.1 to 2.5×10^{-12} m^2 with an arithmetic mean of 1.1×10^{-12} m^2 and a geometric mean of 0.5×10^{-12} m^2. In the fault zone, a zone of increased permeability associated with the GDF, permeability values ranged from 8.5 to 11.1×10^{-12} m^2 and had arithmetic and geometric means of 10.0×10^{-12} m^2. The permeability values of the footwall ranged from 0.2 to 2.1×10^{-12} m^2 with an arithmetic mean of 1.0×10^{-12} m^2 and a geometric mean of 0.7×10^{-12} m^2. Comparison of the permeability values from borehole NAD-GTB#1a to the Tptpmn permeability values from the surface-based testing program (0.37 to 2.7×10^{-12} m^2) indicated that the permeability values for the hanging wall and the footwall are in the same range as the surface-based values, while the fault-zone permeability values are several factors larger. The higher permeability values of the fault-zone may be due to increased fracturing associated with the GDF.

Cross-hole air-injection tests were done between the three boreholes drilled from the NDR. Analysis of the pressure responses in the monitor intervals identified three zones where the monitor intervals had different pressure responses. These three zones corresponded to the structural units: footwall, fault zone, and hanging wall; the fault zone corresponds to the intensely fractured zone that extended from the main trace of the GDF 1 m into the footwall and 3 m into the hanging wall. Pressure responses did not change with direction. The type-curve analysis indicated a heterogeneous flow system that had three different homogeneous isotropic structural units corresponding to the footwall, fault zone, and hanging wall. The arithmetic mean permeability and porosity values of the three structural units are: footwall 8.7×10^{-12} m^2, and 0.04; fault zone 18.1×10^{-12} m^2, and 0.13; hanging wall 5.0×10^{-12} m^2, and 0.04. Comparison of

the cross-hole permeability values from the NDR to the single-hole permeability values from borehole NAD-GTB#1a indicated close agreement between the arithmetic means for the fault zone (values within a factor of 2) but differences approaching a factor of 5 in the hanging wall and almost an order of magnitude in the footwall. The permeability differences may be real or they may be a scale effect due to the smaller test scale of the single-hole GTB#1a testing. The cross-hole permeability values from the NDR are larger than the permeability values from the surface-based testing of the Tptpmn. The increased permeability is probably due to increased fracturing associated with the GDF.

A numerical model of the northern GDF flow system was developed using the USGS finite-difference model AIR3D. The model incorporated the geologic information from the detailed line survey (DLS), geologic mapping, visual inspection of the NAD and NDR, and borehole video logs. Pressure responses from the numerical model were visually compared to the pressure responses from the field tests. By using these comparisons, the model permeability and porosity values were adjusted, the model was rerun, and the simulated pressure responses again compared to the pressure responses from the field tests. The numerical model estimates of the permeability and porosity values were: footwall 10.0×10^{-12} m^2, and 0.07; fault zone 20.0×10^{-12} m^2, and 0.20; hanging wall 5.0×10^{-12} m^2, and 0.05. These values are very similar to the analytical type-curve values and indicate agreement between the two methods.

Following the type-curve and the AIR3D numerical analysis, a discrete-feature network (DFN) model of the NGDFA was developed using the computer code FRACMAN. The DFN analysis used the forward modeling approach of FRACMAN to develop a three-dimensional DFN model. The approach derived the geometry and spatial distributions of the fracture system used in the model from the DLS and the fracture data from the NAD and NDR. Following the development of the fracture system, transmissivity values were assigned to the fractures. The initial transmissivity values were derived from the permeability values from the type-curve and AIR3D analysis of the cross-hole air-injection tests. The transmissivity values were adjusted and the model was rerun until the simulated pressure responses from the DFN model were similar to the pressure responses from the cross-hole air-injection field tests. The simulated pressure responses from the DFN model were a close match with the field-test pressure responses from the hanging wall and footwall but not a close match with the field-test pressure responses from the fault zone. The pressure responses in the fault zone from the DFN model were generally higher than the pressure responses in the fault zone from the field tests; this may be because the high fracture density of the fault zone is better simulated as an equivalent porous medium.

Cross-hole convergent-tracer tests were done between intervals that had cross-hole pneumatic connections. The cross-hole tracer tests were analyzed using type curves. The initial type-curve analysis ignored the diffusion process because diffusion was assumed to be minimal on the rising limb of the breakthrough curve. Peclet numbers ranged between 3 and 22 with a single test resulting in two Peclet numbers of 80. Advective traveltime ranged from 0.011 to 1.110 days. Transport-porosity values ranged from 0.001 to 0.070. Longitudinal-dispersivity values ranged from 0.06 to 2.63 m. Testing indicated no preferential He diffusion nor SF_6 absorption. Tracer tests done in the footwall of the GDF had transport-porosity values that ranged from 0.003 to 0.032 with an average of 0.013. Tracer tests done in the fault zone had transport-porosity values that ranged from 0.004 to 0.034 with an average of 0.014. Tracer tests done in the hanging wall had transport-porosity values that ranged from 0.001 to 0.070 with an average of 0.013. The large range in transport-porosity values may indicate that the test scale was smaller than the representative elementary volume. The tracer tests did not indicate any directional control; slow and fast tracer transport pathways occur in the same direction and plunge.

The MAFIC computer code, combined with the DFN model, was used to simulate the cross-hole tracer tests. Because of the small test scale (<10 m) and short transport times (<200 minutes) diffusion was assumed to be negligible. As expected, the simulated tracer-arrival plots were close matches with the tracer arrival plots from the field tests done in the hanging wall and the footwall but not in the fault zone. As identified in the DFN cross-hole air-injection model, the intense fracturing in the fault zone is not adequately represented by the DFN model. Particle tracking using the MAFIC code identified flow paths that were as much as six times longer than the linear distance. The long, tortuous flow paths are a partial explanation for the high transport-porosity values (up to 0.070) compared

to the true fracture porosity that usually ranges between 10^{-5} and 10^{-2}. The variability in the length of the flow paths also indicated that a drawn-out arrival-time tail may not be a result of matrix diffusion but could be the result of a complex, variable, nonlinear tracer-transport route.

Although some limitations were identified in dealing with intensely fractured zones, the DFN model indicated that pressure tests and tracer tests done in the hanging wall and footwall of the GDF can be accurately simulated using data from fracture mapping. By using the DFN model, it may be possible to increase the scale of the simulations to determine traveltimes at larger dimensions for areas that have similar fracture networks as the fracture networks of the hanging wall and footwall of the GDF.

REFERENCES CITED

Bear, Jacob, 1972, Dynamics of fluids in porous media: New York, American Elsevier Publishing Co., 764 p.
NNA.19911127.0046

Bear, Jacob, 1979, Hydraulics of groundwater: New York, McGraw-Hill, 569 p.
NNA.19890906.0184

Dershowitz, W., Lee, G., Geier, J., Hitchcock, S., and La Pointe, P.R., 1994, FRACMAN version 2.5—Interactive discrete feature data analysis, geometric modeling and exploration simulation: Redmond, Wash., Golder Associates, Inc. User Documentation, 171 p.
MOL.19970310.0091

Earlougher, R.C., 1977, Advances in well test analysis: Society of Petroleum Engineers Monograph Series, Millet the Printer Inc., Dallas, Texas, 264 p.
NNA.19900104.0471

Fahy, M.F., 1997, Dual-porosity analysis of conservative tracer testing in saturated volcanic rocks at Yucca Mountain in Nye County, Nevada: International Journal of Rock Mechanics and Mining Science, v. 34, no. 3–4, paper no. 074, 5 p.
MOL.19980211.0272

Freeze, R.A., and Cherry, J.A., 1979, Groundwater: Prentice-Hall Inc., Englewood Cliffs, N.J., 604 p.
TIC#3476

Fritz, P., and Fontes, J. Ch., 1980, Handbook of environmental isotope chemistry: Amsterdam, Elsevier Scientific Publishing Co., 545 p.
TIC#243187

Gelhar, L.W., Welty, Claire, and Rehfeldt, K.R., 1992, A critical review of data on field-scale dispersion in aquifers: Water Resources Research, v. 28, no. 7, p. 1955–1974.
MOL.19980514.0053

Hvorslev, M.J., 1951, Time lag and soil permeability in ground-water observations: Vicksburg, Miss., U.S. Army Corps of Engineers, Waterways Experiment Station, Bulletin 36, 50 p.
TIC#238956

Joss, C.J., and Baehr, A.L., 1995, Documentation of AIR3D, an adaptation of the ground-water-flow code MODFLOW to simulate three-dimensional air flow in the unsaturated zone: U.S.Geological Survey Open-File Report 94–533, 154 p.
MOL.19990706.0174

LeCain, G.D.,1995, Pneumatic testing in 45-degree-inclined boreholes in ash-flow tuff near Superior, Arizona: U.S. Geological Survey Water-Resources Investigations Report 95–4073, 27 p.
MOL.19960715.0083

LeCain, G.D., 1997, Air-injection testing in vertical boreholes in welded and nonwelded tuff, Yucca Mountain, Nevada: U.S. Geological Survey Water-Resources Investigations Report 96–4262, 33 p.
MOL.19980310.0148

LeCain, G.D., 1998, Results from air-injection and tracer testing in the upper Tiva Canyon, Bow Ridge Fault, and upper Paintbrush contact alcoves of the exploratory studies facility, August 1994 through July 1996, Yucca Mountain, Nevada: U.S. Geological Survey Water-Resources Investigations Report 98–4058, 28 p.
MOL.19980625.0344

McDonald, M.G., and Harbaugh, A.L., 1988, A modular three-dimensional finite-difference ground-water flow model: U.S. Geological Survey Techniques of Water-Resources Investigations, book 6, chap. A1, 586 p.
NNA.19870729.0113

Miller, I. Lee, G., Dershowitz, W., and Sharp, G., 1994, Matrix/fracture interaction code (MAFIC) with solute transport: Redmond, Wash., Golder Associates, Inc., User Documentation version ß1.4, 58 p.
MOL.19961122.0411

Moench, A.F., 1995, Convergent radial dispersion in a double-porosity aquifer with fracture skin—Analytical solution and application for a field experiment in fractured chalk: Water Resources Research, v. 31, no. 8, p. 1823–1835.
TIC#233132

Ramey, H.J., 1982, Well-loss function and the skin effect—A review: Geologic Society of America, Special Paper 189, p. 265-271.
TIC#245159

Rattray, G.W., Striegl, R.G., and Yang, I.C., 1995, Adsorption of sulfur hexafluoride onto crushed tuffs from the Yucca Mountain Area, Nye County, Nevada: U.S. Geological Survey Water-Resources Investigations Report 95-4057, 29 p. MOL.19970331.0042

Theis, C.V., 1935, The relation between the lowering of the piezometric surface and the rate and duration of discharge of a well using ground-water storage: American Geophysical Union Transcript no. 16, p. 519-524. NNA.19870729.0100

	Data description	Data tracking number	QA status
1.	Borehole video and caliper logs GTB#1a	LARO831422AQ97.001	Q
2.	Borehole video and caliper logs MF#1, 2, and 3	LARO831422AQ97.002	Q
3.	BOR Detailed Line Survey of the NAD and NDR	GS970808314224.014	Q
4.	Geothermal logs GTB#1a	GS970383122410.005	Q
5.	Pneumatic monitoring GTB#1a	GS970283122410.003	Q
6.	Gas-phase chemistry GTB#1a	GS970283122410.002Q	Q
7.	Gas-phase chemistry MF#1	GS981283122410.006	Q
8.	Gas-phase chemistry MF#2	GS981283122410.006	Q
9.	Tritium data GTB#1a (USGS)	GS970283122410.002	[1]non-Q
	do	GS990183122410.001	[1]non-Q
10.	Tritium data MF#1 (U of Miami)	GS990183122410.004	[1]non-Q
11.	GTB#1a, single-hole air-k	GS970383122410.004	Q
12.	2-D air-injection tests	GS980183122410.001	Q
13.	3-D air-injection tests	GS981183122410.005	Q
14.	2-D tracer tests	GS980283122410.003	Q
15.	3-D tracer tests	GS981183122410.005	Q

Computer software identification numbers

1. AIR3D, U.S.Geological Survey documented computer code: ESP 22.01
2. CLUSTRAN, Bureau of Reclamation documented computer code: ESP 5.21
3. FRACMAN, Golder and Associates documented computer code: ESP 14.01

[1]non-Q, non-quality-assured data.

☆ U.S. GOVERNMENT PRINTING OFFICE: 2000 — 573-082 / 47016 Region No. 8